

Towards net-zero manufacturing: carbon-aware scheduling for GHG emissions reduction

Andrea Mencaroni ^{*,a,b}, Pieter Leyman^{a,b}, Birger Raa^a, Stijn De Vuyst^{a,b}, and Dieter Claeys^{a,b}

^aDepartment of Industrial Systems Engineering and Product Design, Ghent University, Ghent, Belgium

^bIndustrial Systems Engineering (ISyE), Flanders Make, Kortrijk, Belgium

Abstract

Detailed scheduling has traditionally been optimized for the reduction of makespan and manufacturing costs. However, growing awareness of environmental concerns and increasingly stringent regulations are pushing manufacturing towards reducing the carbon footprint of its operations. Scope 2 emissions, which are the indirect emissions related to the production and consumption of grid electricity, are in fact estimated to be responsible for more than one-third of the global GHG emissions. In this context, carbon-aware scheduling can serve as a powerful way to reduce manufacturing's carbon footprint by considering the time-dependent carbon intensity of the grid and the availability of on-site renewable electricity.

This study introduces a carbon-aware permutation flow-shop scheduling model designed to reduce scope 2 emissions. The model is formulated as a mixed-integer linear problem, taking into account the forecasted grid generation mix and available on-site renewable electricity, along with the set of jobs to be scheduled and their corresponding power requirements. The objective is to find an optimal day-ahead schedule that minimizes scope 2 emissions. The problem is addressed using a dedicated memetic algorithm, combining evolutionary strategy and local search.

Results from computational experiments confirm that by considering the dynamic carbon intensity of the grid and on-site renewable electricity availability, substantial reductions in carbon emissions can be achieved.

Keywords – Carbon-aware scheduling, Evolutionary computing, Scheduling, Sustainability

1 Introduction

Amid the global push towards net-zero greenhouse gas (GHG) emissions [23], the energy supply sector, being the largest contributor with over one third of total GHGs [36], is set for an unprecedented transformation. While the ever-growing deployment of renewable energy sources is a crucial step in the EU's

*Corresponding author. *E-mail*: andrea.mencaroni@ugent.be

path to net-zero [20], it alone is not sufficient. The inherent variability in renewable energy availability necessitates addressing the demand side as well, making a shift towards supply-driven energy consumption inevitable [22].

Energy is fundamental to all sectors of the economy, from transport to households, agriculture, and industry. With the latter accounting for roughly one fourth of total EU energy consumption in 2022 [21], how energy is generated becomes particularly critical for emissions reduction. GHG emissions are categorized in three scopes: scope 1, which regards direct emissions from owned or controlled sources; scope 2, covering indirect emissions from the generation of purchased electricity, and scope 3, which encompasses all other indirect emissions from an organization’s value chain (i.e., its upstream and downstream activities) [30]. The mix of energy sources used to produce purchased electricity directly affect scope 2 emissions and, consequently, has a major impact on a company’s overall carbon footprint.

In a typical manufacturing environment, electricity is supplied by a combination of on-site renewable utility systems and the public grid [6]. While using on-site renewables is preferable due to their zero scope 2 emissions [31], their availability is limited and subject to variability [5]. In contrast, grid electricity can be considered effectively unlimited in capacity because external balancing mechanisms ensure that supply matches demand. This is achieved by adjusting the generation mix – i.e., varying the contribution of different energy sources such as natural gas, coal, and nuclear power – to meet the real-time electricity needs [1]. As a result, grid electricity’s scope 2 emissions vary over time, leading to time-dependent carbon intensity [44]. Therefore, there is substantial potential to reduce GHG emissions by aligning electricity consumption with the availability of on-site renewable electricity and the grid’s carbon intensity [39].

Hence, the following question naturally arises: *how* can industry optimally respond to fluctuations in grid carbon intensity and renewable electricity availability, thereby decreasing GHG emissions? Carbon-aware scheduling emerges as a promising answer to this research question.

1.1 Overview of the state-of-the-art

Scheduling refers to the well-known decision-making process of allocating resources to tasks over given time periods to optimize one or more objectives [50]. Given the complexity of the process, scheduling has traditionally been modeled as an optimization problem subject to constraints. Many different formulations of scheduling problems exist, reflecting the resource configuration and the nature of the tasks to be scheduled [4]. One of the most common formulations is the permutation flow-shop scheduling problem (PFSP) [26]. With a PFSP model, machines are arranged in series, and the sequence of jobs on machines is maintained across all the machines. The popularity of PFSP lies in the fact that this configuration resembles how assembly lines are built, where semi-finished products are moved through subsequent workstations

by means of conveyor systems. Since the 1960s, the practical relevance of PFSP has drawn considerable research attention. However, the predominant focus has been on minimizing makespan [2, 48]. While optimizing for faster production has driven industrial development for decades, this objective no longer fully aligns with the current context of environmental concerns. The global energy crisis of 2021, which triggered record-high energy prices [34], accelerated a shift in research focus toward minimizing energy costs by incorporating dynamic electricity pricing. While many studies have addressed the reduction of energy costs, often in combination with makespan minimization, the majority have relied on fixed time-of-use (TOU) pricing strategies (e.g., [9, 10, 12, 13, 29, 32, 37, 43, 45–47, 49, 51–53, 57, 58]). Few studies considered real-time pricing (RTP), where electricity prices vary throughout the day without predefined tariffs (e.g., [15, 25, 55]). However, although such pricing strategies often reduce demand variance, there is no clear evidence that this reduction consistently leads to lower emissions [33].

Although some studies have considered simultaneous minimization of makespan and carbon emissions, the majority relied on annual average carbon emission factors (e.g., [14, 16, 24, 28, 40, 41]), neglecting the time-dependent variations in grid carbon intensity. Only very few have addressed the time-dependent nature of grid carbon intensity. For instance, Zhang et al. [60] proposed a flow-shop scheduling model to minimize total energy costs and carbon emissions by incorporating dynamic grid carbon intensity and TOU energy prices. Similarly, Kelley et al. [38] developed a single-machine scheduling model to minimize GHG emissions using hourly grid generation mix data. Lastly, Trevino-Martinez et al. [56] introduced a single-machine scheduling model to jointly minimize total energy and carbon emissions costs by incorporating a carbon tax. However, all these studies omitted on-site renewable generation and did not present an algorithm capable of solving real-world sized instances. To the best of our knowledge, no study has yet delivered a ready-to-use, practical scheduling algorithm that minimizes GHG emissions while simultaneously considering time-dependent grid carbon intensity, on-site renewable generation, and job power requirements.

1.2 Scope of the paper

To address the identified research gap, this study proposes a permutation flow-shop carbon-aware scheduling model aimed at minimizing scope 2 GHG emissions in manufacturing. The problem is formulated as a Mixed-Integer Linear Program (MILP) and solved using a novel memetic algorithm, which integrates evolutionary computing with local search.

The key contributions of this study are three-fold. First, it integrates time-dependent grid carbon intensity, on-site renewable electricity generation, and dynamic job power requirements into the model, enabling carbon-aware scheduling. Second, it reflects real-world manufacturing constraints by formulating

the problem within a PFSP environment, which closely resembles traditional production lines. Finally, the proposed algorithm finds high-quality solutions for real-world-sized instances within short computation times, making it suitable for practical applications.

The remainder of this paper is structured as follows. In Section 2, the model and the associated terminology are introduced. Then, in Section 3, the components and parameters of the memetic algorithm are described. Next, in Section 4, computational experiments are presented and discussed. Finally, conclusions and directions for future research are outlined in Section 5.

2 Model formulation

We now introduce the carbon-aware scheduling model by following two steps. In Section 2.1, we first introduce the concept of time-dependent job power requirements and present the methodology for computing grid carbon intensity. Then, in Section 2.2, we present the mathematical formulation of the MILP model, including the relevant terminology and underlying assumptions.

2.1 Job power requirements and grid carbon intensity

Traditionally, time has been considered the primary resource required to process jobs on machines. However, manufacturing operations also depend on electrical power, whose demand may vary throughout a job’s execution. For instance, certain tasks may involve a machine warm-up phase, typically resulting in ramp-up or ramp-down power profiles. Figure 1 illustrates five example jobs with their corresponding processing times and power requirement profiles.

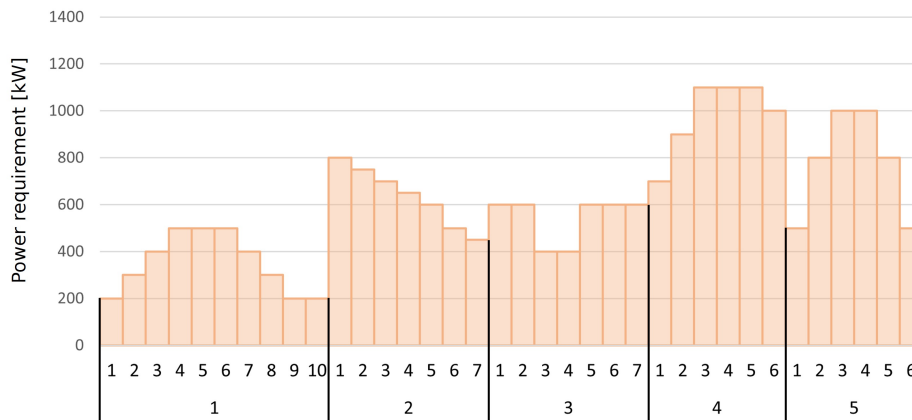


Figure 1: Example of five jobs with corresponding processing time and power requirements

The source of electricity used to power machines significantly impacts GHG emissions. In this model, two possible sources of electrical power are considered: on-site renewable generation and the public grid.

On-site renewable power includes installations such as photovoltaic (PV) systems, wind turbines, and

heat recovery stations. Electricity generated from these sources is preferable as it does not contribute to scope 2 GHG emissions. However, on-site renewable power is typically limited in capacity and fluctuates throughout the day depending on external factors such as the weather conditions.

The second source is electricity from the public grid. Unlike on-site renewable power, the grid provides a virtually unlimited supply, supported by external balancing systems that ensure demand is met at any moment of the day. However, electricity from the grid is associated with scope 2 GHG emissions, as its production often relies on carbon-intensive energy sources. These emissions are typically expressed in grams of carbon dioxide equivalent (gCO₂eq), a standardized unit that accounts for the global-warming potential (GWP) of different greenhouse gasses.

The GHG emissions per unit of grid electricity, which are referred to as grid carbon intensity, can be estimated based on the generation mix and the lifecycle emissions of each contributing energy source, which are summarized in Table 1.

Source	Lifecycle emissions in gCO ₂ eq/kWh (Min/Median/Max)
Pulverized coal	740/ 820 /910
Gas – Combined cycle	410/ 490 /650
Biomass – cofiring	620/ 740 /890
Biomass – dedicated	130/ 230 /420
Geothermal	6/ 38 /79
Hydropower	1/ 24 /2200
Nuclear	3.7/ 12 /110
Concentrated Solar Power	8.8/ 27 /63
Solar PV – rooftop	26/ 41 /60
Solar PV – utility	18/ 48 /180
Wind onshore	7/ 11 /56
Wind offshore	8/ 12 /35

Table 1: Emissions of selected electricity supply technologies, reprinted from [35]

By calling G the amount of possible energy sources and θ_g the median lifecycle emission factor of source g , the grid carbon intensity at time period j can be calculated as:

$$C_j = \sum_{g=1}^G w_j^g \theta_g \quad , \quad (1)$$

where w_j^g is the share of energy source g in the generation mix in period j , computed as:

$$w_j^g = \frac{Q_j^g}{\sum_{h=1}^G Q_j^h} \quad , \quad (2)$$

and Q_j^g is the contribution of energy source g to the grid generation mix in period j . Note that the

this formulation expresses C_j as a weighted sum of the lifecycle emission factors θ_g , where the weights correspond to the shares of each energy source in the generation mix in period j .

Although the actual generation mix shifts throughout the day due to real-time adjustments for unexpected fluctuations in supply and demand, system operators establish day-ahead generation schedules that account for economic and technical constraints for plant operations. Figure 2 illustrates the day-ahead generation schedule for a representative day in Belgium, showing the planned generation mix and corresponding carbon intensity. The carbon intensity, shown on the secondary y-axis, fluctuates significantly throughout the day due to varying generation sources. For instance, during peak demand periods, a higher reliance on natural gas often results in increased carbon intensity.

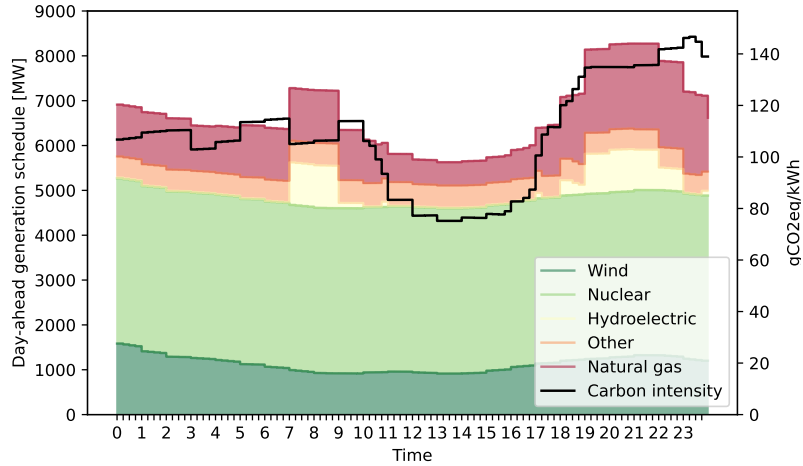


Figure 2: Grid carbon intensity and power generation mix

2.2 Carbon-aware scheduling model

After discussing the time-dependent nature of job power requirements, the possible energy sources, and the methodology for computing grid carbon intensity, we now formally introduce the carbon-aware permutation flow-shop scheduling model.

Consider a set of N jobs to be processed on M machines over a planning horizon divided into T equal time periods j , with $j \in \{1, \dots, T\}$. Each job $i \in \{1, \dots, N\}$ consists of M operations O_i^m , where $m \in \{1, \dots, M\}$, to be executed sequentially on the machines in a non-preemptive manner. The sequence of jobs is identical across all machines, following the permutation flow-shop constraint. Each operation O_i^m has a specific processing time of D_i^m periods and requires a defined amount of electrical power P_{ik}^m per period, with $k \in \{1, \dots, D_i^m\}$.

This electricity can be sourced either from on-site renewable energy or from the public grid. Electricity generated from on-site renewable sources is free of scope 2 GHG emissions, but its availability is both limited and time-dependent. While on-site generation is inherently uncertain due to weather variability,

planning typically relies on forecasted availability. Based on these forecasts, the available renewable electricity in period j , denoted by A_j , is assumed to be deterministic and known for the entire planning horizon. Energy storage and feed-in of surplus electricity to the public grid are not permitted, meaning that any available renewable power is directly used to meet the schedule's electricity demand. When on-site renewable power is insufficient, the additional electricity required is drawn from the public grid.

Unlike renewable power, grid electricity has no availability constraints. However, its carbon intensity C_j fluctuates over time based on the generation mix. In this model, deterministic forecasts of the generation mix for the upcoming planning horizon are assumed to be available, allowing C_j to be calculated using Equation (1).

To facilitate the calculation of emissions reduction due to the use of on-site renewables later, we further define:

$$E_{ij}^m = \sum_{k=1}^{D_i^m} P_{ik}^m C_{j+k-1} \quad , \quad (3)$$

as the scope 2 GHG emissions of scheduling operation O_i^m to start in time period j if only grid electricity is used.

Finally, we define the decision binary variables of the models x_{ij}^m , which equal 1 if operation O_i^m is scheduled to start at the beginning of period j , and 0 otherwise.

Before moving on to the MILP formulation, we summarize the assumptions under which the model is formulated:

- a) Job processing times and power requirements are deterministic and known for the upcoming planning horizon. This is a justifiable assumption because manufacturing processes often have well-defined duration and power profiles, especially in controlled production environments. Historical data or dry runs can provide reliable estimates.
- b) On-site renewable power generation is deterministic and known for the upcoming planning horizon. Renewable power generation can be accurately forecasted using weather data and historical generation patterns. While small deviations will exist, day-ahead predictions should be reliable for planning purposes.
- c) Grid generation mix is deterministic and known for the upcoming planning horizon. This assumption is reasonable because generation schedules are typically planned in advance to coordinate the operation of power plants ensuring enough time to start and stop generation to meet the expected demand. These schedules are used to provide accurate forecasts of the grid carbon intensity.
- d) On-site renewable power cannot be stored or injected into the public grid. Therefore, whenever

available, it will be used first. This assumption aligns with scenarios where storage infrastructure is unavailable or uneconomical, and is considered for the sake of simplicity.

The MILP formulation is finally presented in Program (4). The objective function (4a) minimizes the scope 2 GHG emissions of the schedule by first calculating the total emissions assuming exclusive use of grid electricity and then subtracting the saved emissions due to the use of on-site generated renewable power. This allows for pre-calculation of the emission matrix E_{ij}^m , which reduces computational overhead. Constraints (4b) and (4c) ensure that all operations are scheduled and completed within the defined time horizon. Constraints (4d) enforce non-preemption, guaranteeing that once an operation starts, it is executed to completion without interruption. Specifically, if job i starts its m -th operation at time j , no other operation can begin on the same machine until period $j + D_i$. Constraints (4e) are the precedence constraints, preventing the next operation on a subsequent machine from starting until the current operation is completed. Constraints (4f), (4g), and (4h) define the dependent variables p_{ij}^m , which express the scheduled power consumption of operation O_i^m in time period j . Constraints (4i) and (4j) determine the total on-site renewable power used by the schedule in each period j , ensuring it does not exceed the available power A_j at that time. Finally, constraints (4k), (4l), and (4m) ensure the same sequence of jobs is maintained across all the machines. Specifically, constraints (4k) and (4l) determine the values of the auxiliary binary variables $s_{ii'}$ based on the job order on the first machine, where $s_{ii'} = 1$ if job i precedes job i' and 0 otherwise. Constraint (4m) then propagates this sequence across all remaining machines. An overview of the used notation is presented in Table 2.

This problem can be solved with exact methods by using commercial solvers such as Gurobi or CPLEX. However, this is only feasible for limited-sized instances. Since an easier variant of this problem, which do not consider limited on-site electricity generation, is already NP-hard for $M \geq 3$ [27], it follows that the proposed problem is also NP-hard, at least for $M \geq 3$. Therefore, efficient solution methods are needed to tackle real-world sized instances promptly. In this paper, we propose a dedicated memetic algorithm, which will be discussed in the next section.

$$\min_{\mathbf{x}} \sum_{m=1}^M \sum_{i=1}^N \sum_{j=1}^T x_{ij}^m E_{ij}^m - \sum_{j=1}^T y_j C_j \quad (4a)$$

$$\text{s.t.} \quad \sum_{j=1}^T x_{ij}^m = 1 \quad \forall i, m \quad (4b)$$

$$\sum_{j=1}^T j x_{ij}^m + D_i^m \leq T \quad \forall i, m \quad (4c)$$

$$x_{ij}^m + T(1 - x_{ij}^m) \geq \sum_{\ell=1}^N \sum_{r=j}^{\min(j+D_i^m, T)} x_{\ell r}^m \quad \forall i, j, m \quad (4d)$$

$$\sum_{j=1}^k x_{ij}^{m-1} \geq \sum_{j=1}^{k+D_i^{m-1}} x_{ij}^m \quad \begin{cases} \forall i \in \{1, \dots, N\} \\ \forall m \in \{2, \dots, M\} \\ \forall k \in \{1, \dots, T - D_i^{m-1}\} \end{cases} \quad (4e)$$

$$p_{i,j+k}^m \leq P_{ik}^m + M(1 - x_{ij}^m) \quad \begin{cases} \forall i, m \\ \forall j \in \{1, \dots, T - D_i^m + 1\} \\ \forall k \in \{1, \dots, D_i^m\} \end{cases} \quad (4f)$$

$$p_{i,j+k}^m \geq P_{ik}^m - M(1 - x_{ij}^m) \quad \begin{cases} \forall i, m \\ \forall j \in \{1, \dots, T - D_i^m + 1\} \\ \forall k \in \{1, \dots, D_i^m\} \end{cases} \quad (4g)$$

$$\sum_{j=1}^T p_{ij}^m \leq \sum_{k=1}^{D_i^m} P_{ik}^m \quad \forall i, m \quad (4h)$$

$$y_j \leq A_j \quad \forall j \quad (4i)$$

$$y_j \leq \sum_{i=1}^N \sum_{m=1}^M p_{ij}^m \quad \forall j \quad (4j)$$

$$\sum_{j=1}^T j x_{ij}^1 \leq \sum_{j=1}^T j x_{i'j}^1 + M(1 - s_{ii'}) \quad \forall (i, i') : i \neq i' \quad (4k)$$

$$\sum_{j=1}^T j x_{ij}^1 \geq \sum_{j=1}^T j x_{i'j}^1 + 1 - M s_{ii'} \quad \forall (i, i') : i \neq i' \quad (4l)$$

$$\sum_{j=1}^T j x_{ij}^m \leq \sum_{j=1}^T j x_{i'j}^m + M(1 - s_{ii'}) \quad \forall (i, i') : i \neq i', \forall m > 1 \quad (4m)$$

$$x_{ij}^m \in \{0, 1\}, \quad \forall i, j, m \quad (4n)$$

$$s_{ii'} \in \{0, 1\}, \quad \forall (i, i') : i \neq i' \quad (4o)$$

$$p_{ij}^m \in \mathbb{R}^+, \quad \forall i, j, m \quad (4p)$$

$$y_j \in \mathbb{R}^+, \quad \forall j \quad (4q)$$

Parameters	Definition
G	Number of grid energy sources $g \in \{1, \dots, G\}$
N	Number of jobs $i \in \{1, \dots, N\}$
T	Length of planning horizon, $j \in \{1, \dots, T\}$
M	Number of machines $m \in \{1, \dots, M\}$
D_i^m	Processing time of operation O_i^m
P_{ik}^m	Electrical power requirements of operation O_i^m , $k \in \{1, \dots, D_i^m\}$
A_j	Available on-site renewable electricity in time period j
θ_g	Median lifecycle emission factor for grid power source g
Q_j^g	Contribution of source g to the generation mix in time period j
w_j^g	Share of energy source g in the generation mix in period j
C_j	Grid carbon intensity in time period j
E_{ij}^m	Scope 2 emissions of scheduling operation O_i^m to start in time period j and using only grid electricity
Decision variables	Definition
x_{ij}^m	Binary variable, equals 1 if operation O_i^m is scheduled to start at the beginning of time period j , else 0
Auxiliary variables	Definition
y_j	Continuous variable, on-site renewable power used in time period j
p_{ij}^m	Continuous variable, amount of electrical power consumed by operation O_i^m in time period j
$s_{ii'}$	Binary variable, equals 1 if job i is scheduled before job i' , with $i \neq i'$, else 0

Table 2: Summary of symbols and their definitions

3 Memetic algorithm framework

We now introduce the novel memetic algorithm designed to efficiently solve the carbon-aware permutation flow-shop scheduling problem (MA-CAS-PFSP). Memetic algorithms are metaheuristics that integrate local search operators within evolutionary computing, leveraging the strengths of each approach.

Evolutionary algorithms, inspired by natural evolution in biology, operate on a population of individuals, which are encoded solutions. Each individual consists of a set of genes, where each gene corresponds to a specific property of the solution. Through evolutionary operations such as crossover, mutation, and selection, new individuals are generated by modifying genetic material inherited from their predecessors. Over successive generations, this process improves the overall fitness of the population. Due to their strong global search capabilities and general applicability, evolutionary algorithms have been successfully applied to a wide range of combinatorial optimization problems, including scheduling.

However, as stated by the No Free Lunch Theorem, no single optimization algorithm is universally superior across all problems [59]. As a result, evolutionary algorithms can exhibit slow convergence towards optimal solutions. In contrast, local search methods leverage problem-specific knowledge to improve solutions through greedy, fine-tuning mechanisms but are prone to getting trapped in local optima [11]. By integrating these complementary strategies, memetic algorithms have demonstrated superior performance in solving complex scheduling problems [17].

3.1 Solution representation

The first step in evolutionary computing is defining a solution representation, which determines what information is contained in an individual and what solution properties correspond to its genes. The solution representation serves as a link between the problem’s real-world context and the algorithm’s abstract problem-solving space. The choice of data structure used for the solution representation is a critical design aspect of evolutionary algorithms, as it can significantly impact the algorithm’s performance and search efficiency. For scheduling problems, solution representations typically focus on encoding only the sequence of operations to be processed on each machine, with the assumption that operations are scheduled to start as soon as possible. In the case of permutation flow-shop scheduling, encoding the sequence of jobs suffices, as operations are processed in the same order on all machines.

However, in carbon-aware scheduling, the solution representation must allow for planned idle times between operations, as delaying the start of an energy-intense task to a period with high on-site power generation can potentially reduce overall GHG emissions. The proposed solution representation therefore consists of two components: 1) a job sequence, representing the order in which operations are processed on all machines, and 2) idle times, specifying planned time units of delay between the completion of one operation and the start of the next.

The importance of this dual representation lies in its ability to decouple the optimization of job sequences from the optimization of idle times. A given job sequence may in fact result in vastly different solutions depending on how idle times are allocated. By explicitly modeling both components, the algorithm can search for high-quality solutions more effectively by adjusting the job sequence and intermediate idle times independently.

To illustrate this concept, consider an example where five jobs must be scheduled on a single machine within a time horizon of 24 hours. Since each job consists of a single operation, the terms *job* and *operation* can be used interchangeably in this context. The duration and power requirements of the jobs are known with a granularity of 15 minutes and are shown in Table 3. Figure 3a shows the Gantt chart and the

i	D_i^1	P_i^1
1	11	[1500, 1500, 1500, 1500, 1500, 1500, 1500, 1500, 1500, 1500, 1500]
2	8	[2000, 2000, 2000, 1900, 1900, 1900, 2000, 2000]
3	13	[1600, 1600, 1600, 1600, 1600, 1600, 1600, 1600, 1600, 1600, 1600, 1600, 1600]
4	8	[1200, 1200, 1200, 1200, 1200, 1200, 1200, 1200]
5	8	[1400, 1400, 1400, 1400, 1400, 1400, 1400, 1400]

Table 3: Jobs processing times and power requirements for a single-machine example

corresponding power requirement profile over time for a 2-4-5-1-3 job sequence, where jobs are processed as soon as possible. This schedule yields a total GHG emission of 7.27 tCO₂. While all the jobs are indeed

completed on time, a considerable amount of slack time is present at the end of the schedule. If this slack time is instead redistributed as planned pauses between the jobs, GHG emissions can be reduced to 5.61 tCO₂ by aligning the power consumption of the schedule with periods of lower grid carbon intensity. The total duration of the jobs is 48 time periods of 15 minutes each, which given the time horizon of 96 periods results in 48 periods of slack time. Figure 3b illustrates how the same job sequence can lead to lower GHG emissions by incorporating the 12-8-9-0-12-7 sequence of pauses (expressed in time periods) between jobs.

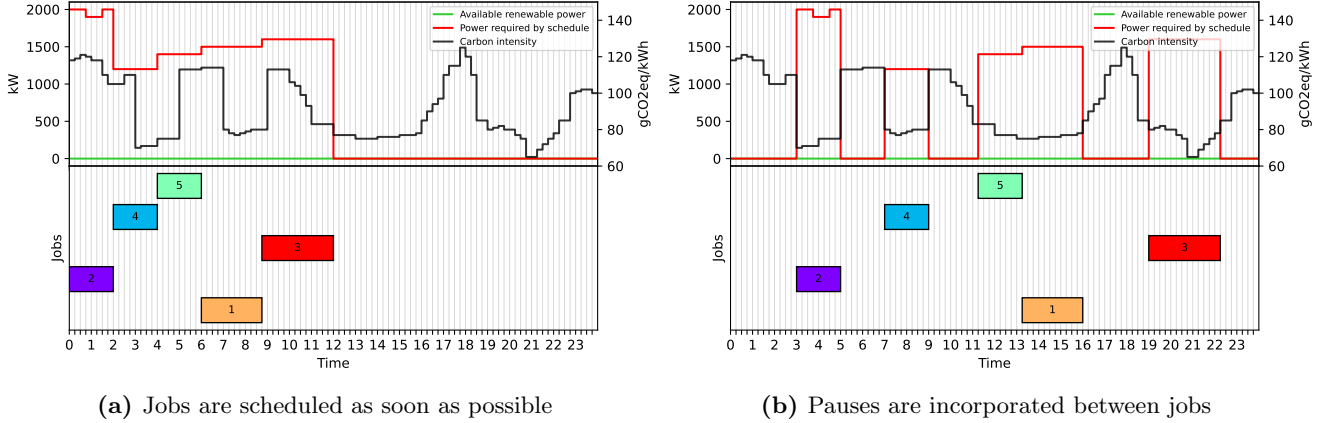


Figure 3: Single-machine example

3.1.1 Encoding and decoding strategy

After defining the solution representation, an encoding and decoding strategy is needed to structure the information in a way that facilitates algorithmic operations. To encode the solution representation, we employ the Random Keys (RK) method [7], where each gene corresponds to a floating-point positive number that indicates scheduling priority between jobs. RKs have been successfully applied to evolutionary algorithms across a wide range of combinatorial optimization problems, particularly in scheduling [42, 54]. A key advantage of RKs is that evolutionary operations such as crossover and mutation between individuals always produce feasible schedules for the first machine, eliminating the need for feasibility checks or repair operators. For the remaining machines, any potential infeasibility can be easily handled in the decoding process without requiring additional repair mechanisms. This benefit will become clearer after the decoding strategy is discussed.

As mentioned earlier, the adopted solution representation consists of two components: the job sequence and the idle times between operations on each machine. Therefore, an encoded solution comprises two parts, one for each component.

The first part corresponds to the job sequence and consists of one array of N RKs, where N is the

total number of jobs. Each RK in this array represents a specific job, with the array elements ordered by the job's index $i \in \{1, \dots, N\}$. These RKs are normalized to sum to one. Normalization mitigates redundancy in solution representation (i.e., multiple encodings representing the same solution), enhancing the algorithm's performance.

The second part of the solution representation consists of M additional arrays, containing information about the pauses between operations on each machine. Each of the M arrays contain $(N + 1)$ RKs, which encode the lengths of pauses before, between, and after the N operations, and is also normalized to one.

The decoding process transforms the RK-based representation into a feasible schedule. This process is performed separately for each of the two parts of the solution representation. First, the job sequence is determined by sorting the job RKs in ascending order. The indices of the jobs, arranged by the increasing value of their corresponding RKs, define the order in which the jobs are scheduled. Next, the idle times between operations are derived by scaling and rounding the pause RKs to match the total slack time of the schedule on machine m , which is precomputed as:

$$S^m = T - \sum_{i=1}^N D_i^m \quad , \quad (5)$$

where T is the total available time and D_i^m is the processing time of operation O_i^m . The RKs in the pause arrays represent thus the proportional distribution of the slack time between consecutive operations. Since idle times must be expressed as integers, a sum-safe rounding strategy is applied during the scaling process. This ensures that the total assigned idle time matches the available slack time S^m exactly, preventing any loss or excess due to rounding errors.

To visualize the decoding process, considering again the single-machine example shown in Figure 3b, where each job consists of only one operation. A possible encoded representation for this example and its corresponding decoded solution are depicted in Figure 4. As shown, the job key array encodes the priority of each job for scheduling. Job 2, having the lowest key value of 0.06, is scheduled first, while job 3, which has the highest key value, is scheduled last. Regarding the idle times, the total slack time of 48 periods is distributed based on the pause key array. The first idle time interval, with a key value of 0.25, is assigned approximately 25% of the total slack time, resulting in 12-period delay before the start of job 2, the first job in the sequence. Similarly, the second idle period, occurring between the end of job 2 and the start of job 4, receives 17% of the slack time.

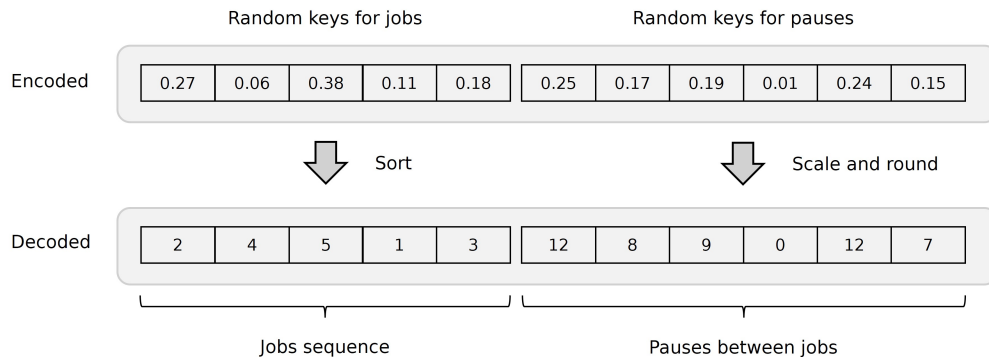


Figure 4: Encoded and decoded individual for the single-machine example of Figure 3b

Once the start times of all the operations are determined by decoding the solution, the fitness of a given individual is calculated by computing the net energy requirements of the schedule at each period $j \in \{1, \dots, T\}$ and then multiplying them by the carbon intensity factor C_j .

As previously mentioned, adopting RKs for solution representation simplifies evolutionary operations by inherently ensuring feasibility on the first machine. Regardless of the individual key values, they can always be sorted to determine a valid job order or scaled and rounded to compute a feasible pause sequence. This eliminates the need for feasibility checks or repair operators, thereby improving algorithm efficiency. In addition, the use of RKs enable effective exploration of high-quality solutions neighborhoods. Even small changes in key values correspond to gradual, incremental adjustments in the decoded solution. This limited redundancy in solution representation enhances the precision of local search, making it particularly effective for refining solutions.

3.2 Initialization and evaluation

The first phase of the algorithm involves creating the first population, consisting of ρ individuals, and calculating their fitness level. First generation's individuals are randomly created by sampling keys for the two types of solution arrays. Job sequence keys are independently sampled from a uniform distribution over the interval $[0, 1]$. Once the array is complete, its keys are normalized to sum up to 1. Pause keys, in contrast, are sampled from an exponential distribution with expectation 1.

The choice of an exponential distribution for pause keys is motivated by the need to increase the probability of larger values, resulting in a more asymmetric allocation of idle times. Each machine $m \in \{1, \dots, M\}$ has a dedicated pause key array, which, after sampling, is normalized and scaled to the available slack time on that machine. This approach results in a more varied spread of idle times between operations compared to a uniform distribution. In particular, it increases the likelihood of generating solutions where idle time intervals occasionally span multiple consecutive periods, which better aligns

with the characteristics of energy-related data, as periods of low on-site renewable generation or high grid carbon intensity often extend over multiple time units.

While the use of RKs guarantees feasibility of the schedule on the first machine, this does not necessarily hold for subsequent machines. Due to precedence constraints between consecutive operations of the same job, a schedule that is feasible on the first machine may cause the time limit T to be exceeded on subsequent machines, making the schedule unfeasible. This is particularly likely when a considerable idle time is planned at the beginning of the schedule. Instead of repairing such infeasible schedules, which would require additional computations, we assign them a penalty for exceeding the maximum time T , proportional to the lateness of the schedule. The evolutionary process of the algorithm will naturally eliminate such low-fitness individuals over successive generations.

To ensure that at least one feasible schedule is present in the initial population, we first generate $\rho - 1$ random individuals and then manually include a single trivial feasible schedule where jobs are processed in a first-come-first-serve (FCFS) sequence with no idle time between operations. While not strictly necessary, this heuristic initialization accelerates convergence with only minimal additional computational overhead. The initialization procedure is then finalized by decoding the individuals and calculating their fitness, resulting in the first current generation of the algorithm.

3.3 Controlled swap uniform crossover

Once the current generation is available – whether from the algorithm’s initialization or the start of a new iteration – the algorithm begins generating a new offspring. The first operation in this process is crossover, where new individuals are generated by recombining the genetic information of parent individuals.

We propose a controlled swap uniform crossover operator. The term uniform refers to the equal probability of selecting non-identical parents from the current generation. Once a pair of parents is chosen, their corresponding keys are swapped to produce two new individuals. This swap is carried out independently for the job sequence key array and the pause key arrays and is controlled by two types of parameters that influence both the frequency and the intensity of the crossover.

The first type is the crossover rate ξ , which determines the proportion of offspring generated through crossover. The remaining $(1 - \xi)\%$ of individuals are selected directly from the current generation using an elitist approach. For example, with a population size of $\rho = 100$ individuals and $\xi = 0.7$, on average, 70 individuals in the offspring will be generated through crossover.

The second type is the crossover probability χ , which dictates the fraction of genes to be swapped between parents within a given array, thereby controlling the severity of the crossover. For instance, with $N = 5$ jobs and $\chi = 0.4$, on average, 2 job keys will be swapped between each pair of parents.

To account for the differing roles of the job sequence array and pause arrays, separate crossover probabilities, χ_j and χ_p , are defined. These parameters independently control the swapping likelihood for the job sequence and the pause keys, respectively.

After swapping, the key arrays are normalized to sum up to one. The generation of two new individuals with the proposed crossover operator is illustrated in Figure 5.

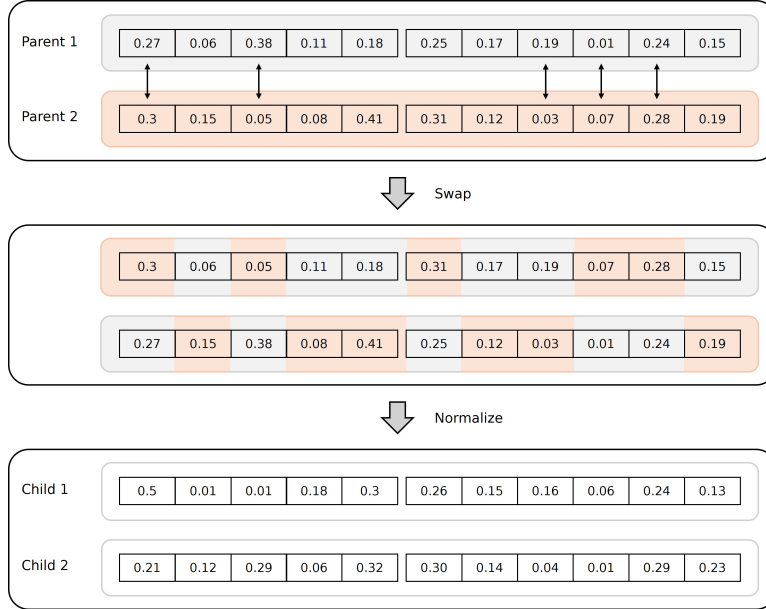


Figure 5: Crossover on a single-machine example with $N = 5$, $\chi_j = 0.4$, and $\chi_p = 0.5$

3.4 Nonuniform mutation

The second operation applied to the newly created offspring is mutation. We employ a nonuniform mutation strategy, where the genes of an individual are modified by adding a random value to its RKs. These random values are independently sampled from a normal distribution with mean of zero and a variable standard deviation: σ_j for the job key array and σ_p for the pause key arrays. These standard deviations, referred to as mutation step sizes, control the severity of the mutation, determining how far the new value deviates from the original one. Smaller step sizes produce mutations closer to the original value, while larger step sizes introduce more significant changes. To ensure all keys remain non-negative after mutation, any resulting negative values are clipped to zero. The key arrays are then again normalized, preserving the consistency of the representation.

Although every individual in the offspring undergoes the mutation process, not all the genes within an individual are necessarily altered. For each individual, the mutation is applied probabilistically to each gene, with the likelihood of mutation determined by the respective mutation probabilities: π_j for the job keys and π_p , for the pause keys. This means that each gene in an individual is independently evaluated

against its mutation probability to decide whether it will be mutated. With these four parameters, the frequency (π_j and π_p) and severity (σ_j and σ_p) of mutation for job sequence keys and pause keys can be independently controlled.

The effect of mutation on a single individual is illustrated in Figure 6, where a single-machine example with $N = 5$ jobs is considered. For the job key array, the mutation probability is $\pi_j = 0.2$, meaning that, on average, 20% of the N RKs – equivalent to one gene in this case – will undergo mutation. The severity of the mutation is controlled by the step size $\sigma_p = 0.06$, indicating that a random value sampled from $\mathcal{N}(0, \sigma_p)$ is added to the selected gene. For the pause key array, the mutation probability is set at $\pi_p = 0.5$, which means that, on average, half of the pause genes – three out of the six in this example – will be mutated. The larger step size of $\sigma_p = 0.2$ results in more significant changes for the mutated pause keys compared to the job keys.

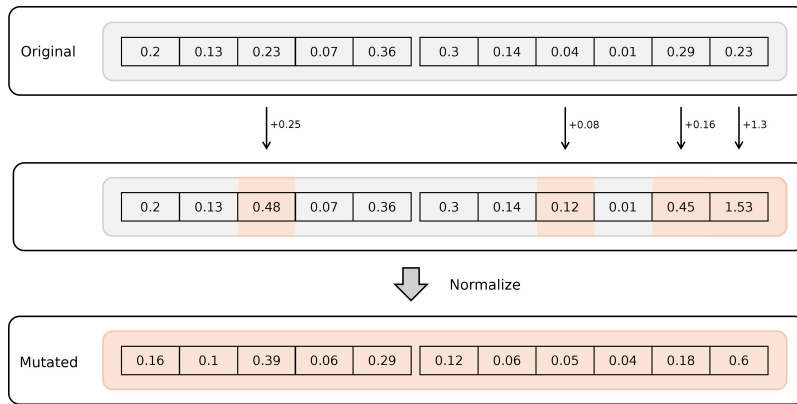


Figure 6: Mutation on a single-machine example with $N = 5$, $\pi_j = 0.2$, $\sigma_j = 0.06$, $\sigma_p = 0.2$, and $\pi_p = 0.5$

3.5 Local search

Next, local search is performed to improve the solution by applying problem-specific knowledge. We adopt a pairwise adjacent swap operator, which iteratively examines adjacent job swaps in the sequence and recalculates the fitness after each swap. The search stops upon finding an improvement, at which point the RKs of the corresponding swap are also exchanged, resulting in an encoded improved solution. Figure 7 shows an example of one possible swap with the proposed local search operator.

3.6 Selection and termination criterion

After crossover, mutation, and local search, the offspring generation is completed. The next step involves combining the current population with the offspring, sorting all individuals by descending fitness, and selecting the top ρ individuals as the new generation. This elitist selection strategy ensures that only the most fit individuals, including any improvements over the current population, are retained. The process



Figure 7: Local search on a single-machine example individual

is repeated until the predefined maximum number of generations γ is reached.

An overview of the proposed MA-CAS-PFSP algorithm framework is presented in Figure 8, while Table 4 summarizes its relevant parameters and their definition.

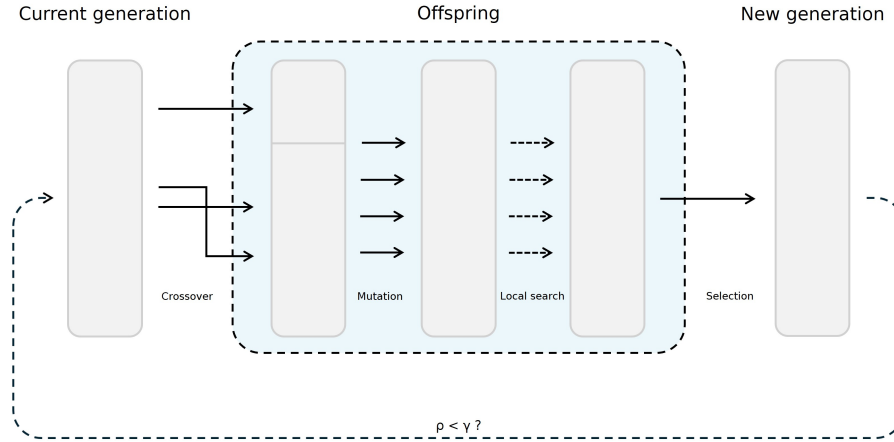


Figure 8: Overview of the proposed MA-CAS-PFSP algorithm

Parameter	Definition
ρ	Population size
γ	Maximum number of generations
ξ	Crossover rate
χ_j	Crossover probability for jobs
χ_p	Crossover probability for pauses
π_j	Mutation probability for jobs
π_p	Mutation probability for pauses
σ_j	Mutation step size for jobs
σ_p	Mutation step size for pauses

Table 4: Summary algorithm parameters and their definitions

4 Computational experiments

We now present and discuss the computational experiments conducted in this study by first detailing the instance dataset generation procedure. Next, we outline the algorithm parameter tuning process. Finally, we discuss the results of computational experiments for both single-machine and multi-machine models.

4.1 Instance dataset

To evaluate the model and compare the algorithm’s performance under varying conditions, a dataset of random instances is required. As benchmarks for carbon-aware scheduling are, to the best of our knowledge, not yet available in the literature, we created a custom dataset of random instances based on historical and self-generated data. An overview of the information stored in each instance is given in Figure 9.

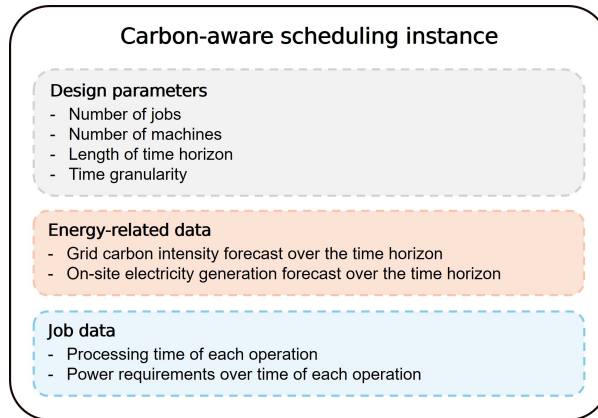


Figure 9: Overview of the information contained in each instance

The instance generation procedure started by defining the experiment design parameters, including the number of machines, the length of the time horizon expressed in planning days, and the time granularity. The creation of the remaining data required for each instance is discussed in the following sections.

4.1.1 Grid carbon intensity forecasts

Grid carbon intensity forecasts were generated using one year of historical generation mix data for the Belgian electricity grid. This dataset, obtained from the Open Data Platform of Elia, the Belgian transmission system operator, provides data at a 15-minute resolution [18]. Median lifecycle emission factors for each power source, as discussed in Section ??, were used to estimate the grid’s carbon intensity over time. The one-year dataset was divided into individual days, allowing random selection of a planning horizon for each instance. The selected data served as the carbon intensity forecast for the instance’s planning horizon. An example of grid carbon intensity profile for one specific day was already shown in

Figure 2, while Figure 10 illustrates an overview of the hourly carbon intensity of the Belgian grid in 2023, which served as input data for this study.

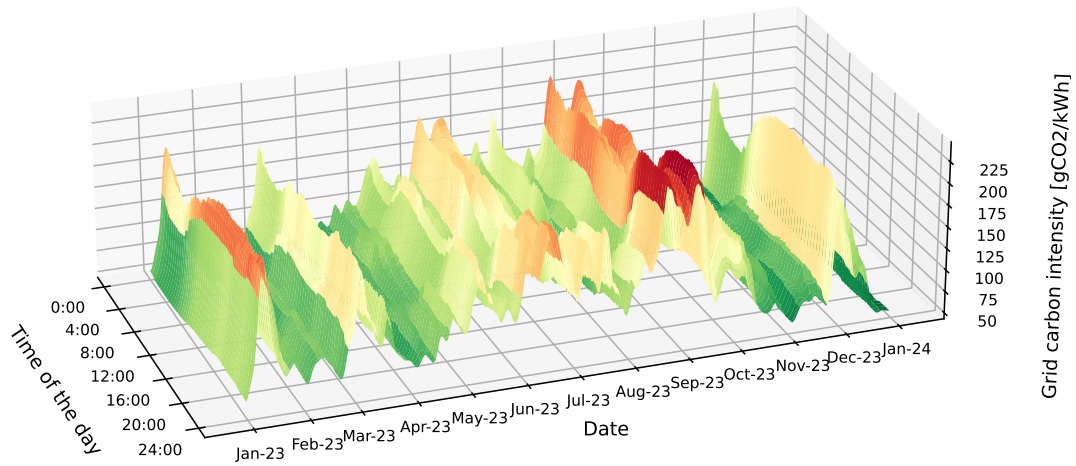


Figure 10: Hourly carbon intensity of the Belgian grid in 2023

4.1.2 On-site electricity generation forecasts

On-site electricity generation forecasts were also sourced from the Open Data Platform of Elia, focusing specifically on solar power generation. Assuming the solar production patterns remain consistent over the years, we used one year of historical solar power generation data as the basis for the forecast. Similar to the grid carbon content, this historical data was treated as forecasts for the planning horizon in each instance [19]. An overview of the hourly on-site generation in Belgium in 2023, which served as input data for this study, is shown in Figure 11.

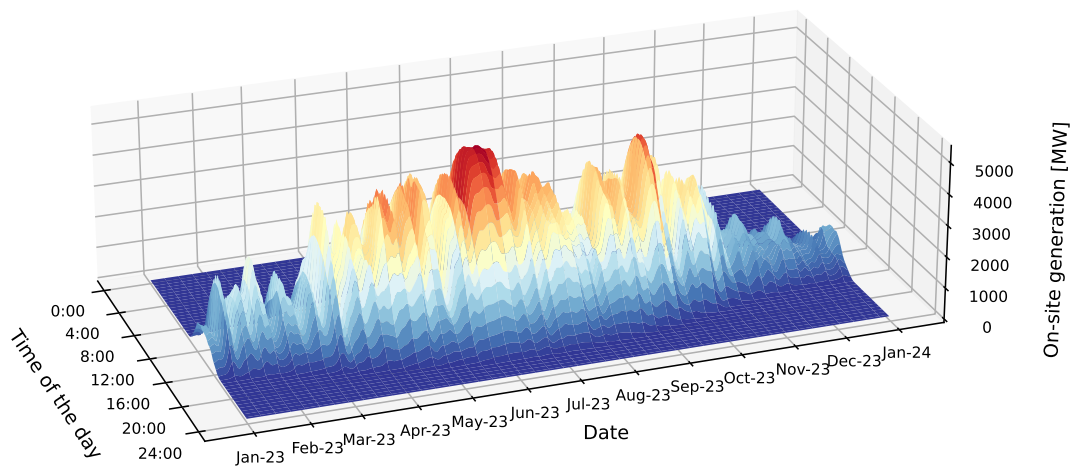


Figure 11: Hourly on-site solar generation in Belgium in 2023

4.1.3 Jobs processing times and power requirements

The generation of job data began with the creation of a pool of available operations. As outlined in Section 2, each job comprises an equal number of operations M , with each operation having its own processing time and power requirements over time.

The processing times of operations, expressed in equal time periods, were sampled from a uniform distribution. Considering the quarter-hour granularity of the available historical data, the sampling intervals were defined as $[2, 16]$ for single-machine instances, and $[0, 8]$ for multiple-machine instances. This approach allows for the inclusion of dummy operations with zero processing time on certain machines for multiple-machine instances, effectively representing jobs that do not require processing on those machines.

While determining the processing times for each operation, power requirements were also assigned. First, a base power requirement was sampled from a uniform distribution within the interval $[100, 3000]$. Subsequently, for each time period of the operation, an individual power requirement was calculated by adding a random value sampled from $\mathcal{U}[-250, 250]$ to the operation’s base power requirement. This approach introduces variability both between operations and across time periods within a single operation, thereby modeling realistic fluctuations in power requirements of jobs.

4.1.4 Instance generation

Once all required data were prepared, individual instances were created. The process began by selecting a random time window from the historical energy-related data, corresponding to the planning horizon T . The selected data provided the grid carbon intensity and on-site generation forecasts for the chosen horizon.

Then, job data was added to the instance by randomly combining operations from the operations pool into jobs, making sure that the time needed to process them did not exceed the available time. The process was repeated until four datasets of fifty random instances each were created. An overview of the instance generation procedure is shown in Algorithm 1. Table 5 summarizes the instance datasets created for the experiments conducted in this study along with their key features.

Name	# instances	M	T	# operations (Min/Median/Max)
CAS-PFSP-M1T1	50	1	96	6/ 10 /15
CAS-PFSP-M1T3	50	1	288	25/ 32 /40
CAS-PFSP-M3T1	50	3	96	24/ 36 /54
CAS-PFSP-M3T3	50	3	288	102/ 135 /183

Table 5: Overview of the instance datasets and their key features

Algorithm 1: Instance generation algorithm

```
Data:  $M, T, \mathbf{C}_{hist}, \mathbf{A}_{hist}$   
Result:  $\mathbf{I}$ : instance dataset  
# Create pool of operations  
 $o \leftarrow 1$   
while  $o < 2000$  do  
  # Sample processing time  
   $D_o \leftarrow$  random draw from  $\mathcal{U}[0, 8]$   
  # Sample power requirements  
   $P \leftarrow$  random draw from  $\mathcal{U}[100, 3000]$   
   $k \leftarrow 0$   
  while  $k < D_o$  do  
     $\Delta P \leftarrow$  random draw from  $\mathcal{U}[-250, 250]$   
     $P_{ok} \leftarrow P + \Delta P$   
     $k \leftarrow k + 1$   
  end  
  Append  $[\mathbf{P}_o]$  to  $\mathbf{O}$   
   $o \leftarrow o + 1$   
end  
# Create instances  
 $n \leftarrow 1$   
while  $n \leq 50$  do  
   $t \leftarrow 0$   
  while  $t < T$  do  
    # Add jobs to instance  
     $i \leftarrow 1$   
    CandidateJob  $\leftarrow []$   
     $m \leftarrow 1$   
    while  $m < M$  do  
      # Pick an operation from the pool  
       $o \leftarrow$  random draw from  $\mathcal{U}[1, 2000]$   
       $O_i^m \leftarrow \mathbf{O}_o$   
      Append  $O_i^m$  to CandidateJob  
       $m \leftarrow m + 1$   
    end  
    # Check feasibility  
     $t_{new} \leftarrow$  FCFS makespan with CandidateJob  
    if  $t_{new} < T$  then  
       $\mathbf{J}_i \leftarrow$  CandidateJob  
       $t \leftarrow t_{new}$   
    end  
     $i \leftarrow i + 1$   
  end  
  # Add energy-related data  
   $d \leftarrow$  random draw from  $\mathcal{U}[1, 365]$   
   $\mathbf{C} \leftarrow \mathbf{C}_{hist}[d : d + T]$   
   $\mathbf{A} \leftarrow \mathbf{A}_{hist}[d : d + T]$   
   $\mathbf{I}_n \leftarrow (\mathbf{J}, \mathbf{C}, \mathbf{A})$   
   $n \leftarrow n + 1$   
end
```

4.2 Parameter tuning

Parameter tuning was performed in Python with Optuna [3], a state-of-the-art open-source hyperparameter optimization framework. Optuna employs Tree-structured Parzen Estimator (TPE) [8], a Bayesian optimization method, to model the performance of different parameter configurations and guide the search towards promising regions of the search space. For each dataset, a representative instance was selected and used to run 1000 trials, with Optuna automatically selecting the parameter setting for each trial. During these trials, the population size was fixed at $\rho = 250$, and the maximum number of generations was set to $\gamma = 100$. The parameter configuration that yielded the best results during the experiment was then identified as the optimal setting for the corresponding dataset. An overview of the results is provided in Table 6.

	CAS-PFSP-M1T1	CAS-PFSP-M1T3	CAS-PFSP-M3T1	CAS-PFSP-M3T3
ξ	0.5812	0.6401	0.6735	0.8784
χ_j	0.2002	0.1291	0.3504	0.1903
χ_p	0.3005	0.2263	0.1278	0.3385
π_j	0.0847	0.005	0.0485	0.0277
π_p	0.1381	0.0375	0.0379	0.011
σ_j	0.0968	0.0051	0.005	0.1533
σ_p	0.1806	0.1822	0.1759	0.1963

Table 6: Overview of the optimal parameter values for each dataset

4.3 Experiments design

The experiments aimed to evaluate the performance and scalability of the proposed MA-CAS-PFSP algorithm across various instance sizes. To achieve this, we conducted four sets of experiments, each corresponding to one of the datasets discussed in Section 4.1.4.

In each experiment, the MA-CAS-PFSP algorithm was executed 10 times on each of the 50 instances within the dataset. Since the search process is inherently random, multiple runs are necessary to ensure variability in the results is effectively captured.

For each instance within a dataset, we report the average and best objective values achieved across the 10 runs of the memetic algorithm, along with the average computation time. To provide a normalized measure of variability in results, the coefficient of variation (CV) is also included, defined as the ratio of the standard deviation to the mean objective value.

The performance of the proposed algorithm is assessed by comparing the results to those generated with the CPLEX implementation of the MILP model presented in Section 2. A time limit of 1 minute was applied to all the experiments on all datasets.

To assess the algorithm’s performance, we define the percentage gap as:

$$\% \Delta = \frac{(\text{Obj}_{\text{CPLEX}} - \text{Obj}_{\text{MA}})}{\text{Obj}_{\text{CPLEX}}} \cdot 100 , \quad (6)$$

where $\text{Obj}_{\text{CPLEX}}$ and Obj_{MA} refer to the best objective values found within the given time limit with CPLEX and MA respectively.

For all experiments, the population size was set to $\rho = 250$ individuals, and the algorithm was terminated after $\gamma = 100$ generations. For the CPLEX results, the best solution found within the specified time limit was recorded for comparison.

All the experiments were conducted on a machine equipped with an 11th Gen Intel(R) Core(TM) i5-1145G7 processor (2.60 GHz), using Python version 3.10.0.rc2.

4.4 Results

We now report the results of the experiments described in Section 4.3, highlighting general trends across the four datasets. For detailed per-instance results, we refer to Tables 8, 9, 10, and 11 in Appendix A.

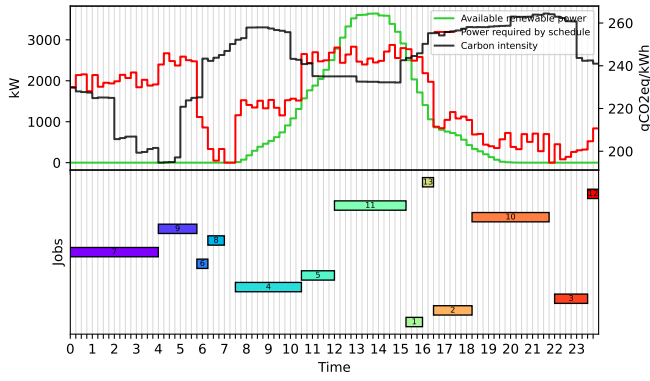
4.4.1 Solution characteristics

Figure 12 illustrates a MA solution for the benchmark instance of each dataset, showing both the Gantt chart and the corresponding power requirement profile. Expectedly, the algorithm consistently schedules jobs such that the resulting power requirements are aligned with moments where either there is sufficient on-site renewable generation, or the carbon intensity of the grid is at its lowest. Depending on the available slack time in each instance, the algorithm may also introduce some planned idle time between operations.

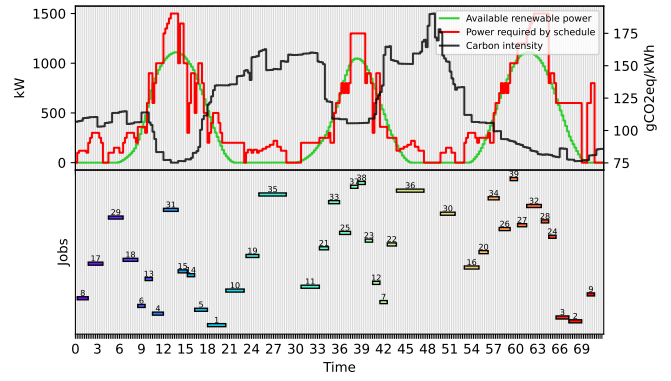
4.4.2 Algorithm performance

Figure 13 provides an overview of the MA’s performance, showing the percentage gap across the four datasets, both per instance and on average.

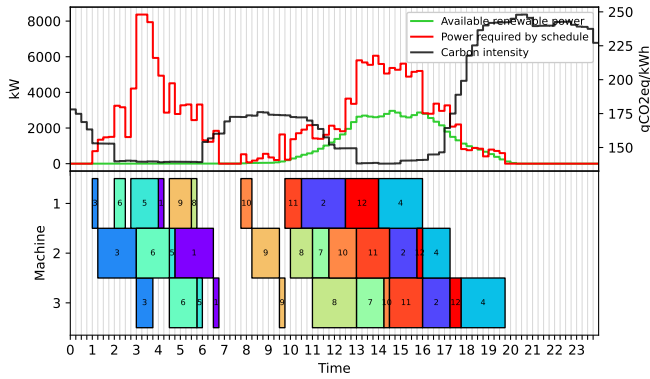
The MA algorithm consistently outperforms CPLEX on all datasets except CAS-PFSP-M1T1 (Figure 13a). This result was expected, as CPLEX found optimal solutions for all instances in this dataset within the 1-minute time limit, making it theoretically impossible for the MA to achieve better results. Nevertheless, the MA reaches optimal solutions in 47 out of 50 instances, with an average computation time of 0.95 seconds, compared to 4.79 seconds for CPLEX. These results confirm the effectiveness of the MA on smaller instances, which serves as a crucial validation step before applying it to larger instances where optimal solutions cannot be obtained with CPLEX.



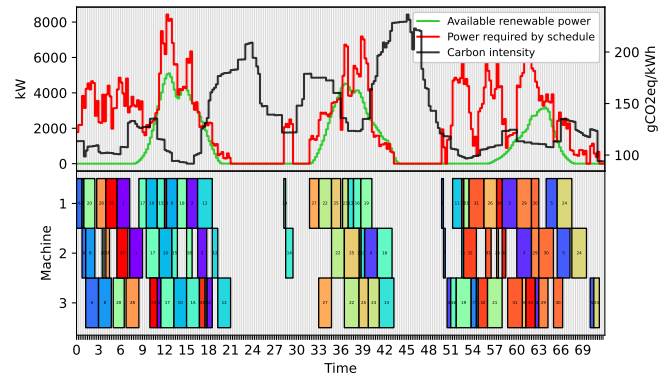
(a) CAS-PFSP-M1T1



(b) CAS-PFSP-M1T3



(c) CAS-PFSP-M3T1

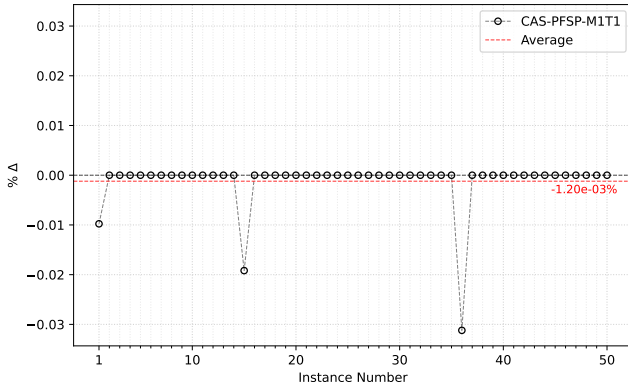


(d) CAS-PFSP-M3T3

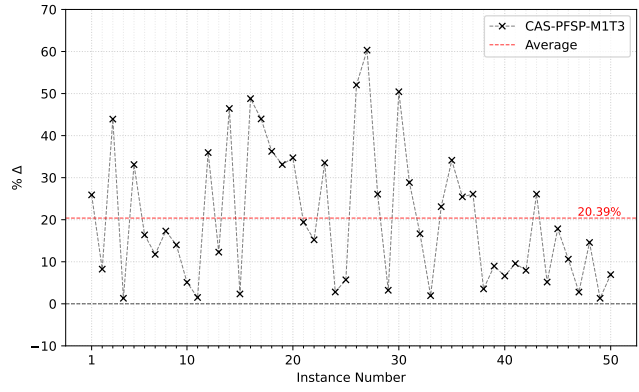
Figure 12: Gantt chart and power requirement profiles for the benchmark instances of each dataset

For the medium-sized M1T3 and M3T1 datasets (Figures 13b and 13c), the MA achieves its highest improvement over CPLEX in the M1T3 dataset, with an average gap of 20.39% compared to 8.95% for M3T1. This difference results from the combinatorial complexity of the instances in these datasets, which is higher in the M1T3 dataset than in the M3T1. In a PFSP scheduling environment, the sequence of the jobs remains fixed across all the machines. Therefore, extending the time horizon (i.e., M1T3 compared to M1T1) has a greater impact on problem complexity than increasing the number of machines (i.e., M3T1 compared to M1T1), which explains the difference in average percentage gaps.

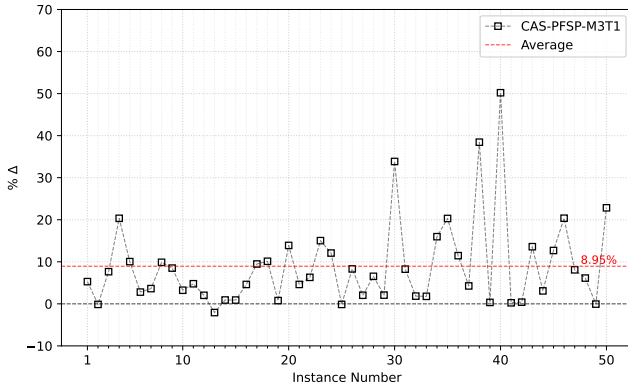
A notable case is the CAS-PFSP-M3T3 dataset, where CPLEX fails to find any integer solution within the time limit. To still provide a reference for performance evaluation, a warm start was given using a FCFS solution. Thus, the percentage gap in Figure 13d represents the MA's improvements over the FCFS schedule.



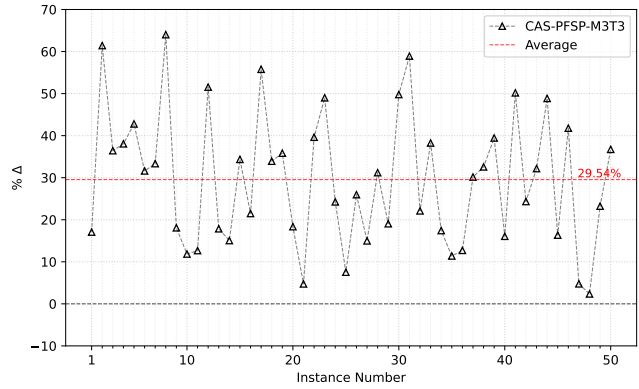
(a) CAS-PFSP-M1T1 dataset



(b) CAS-PFSP-M1T3 dataset



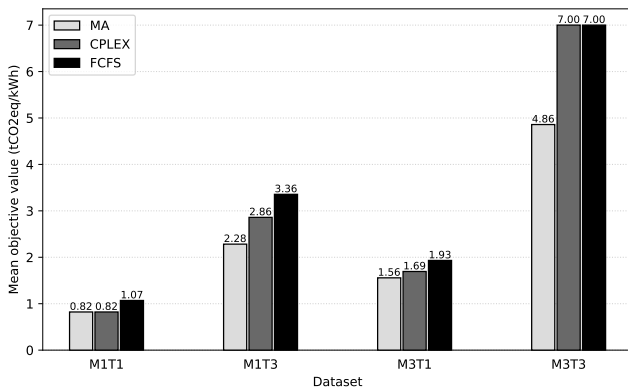
(c) CAS-PFSP-M3T1 dataset



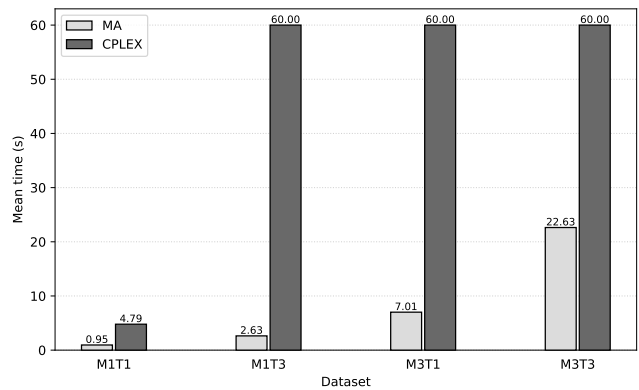
(d) CAS-PFSP-M3T3 dataset

Figure 13: Overview of percentage improvement per instance, per dataset

Figure 14a presents the average objective value across all instances for each dataset. Consistent with the previous discussion, performance gain in average objective value correlates with dataset complexity, highlighting the MA's strong scalability compared to CPLEX. Figure 14b illustrates the average computation times. Detailed results can be found in Appendix A.



(a) Objective value



(b) Computational time

Figure 14: Average performance across each dataset per solution method

4.4.3 GHG emissions reduction

To quantify the reduction in GHG emissions achieved with the proposed method, we compare the obtained solutions against the corresponding FCFS schedules for each instance. Table 7 provides an overview of the results across all instances within each dataset, reporting the minimum, average, and maximum percentage reduction in GHG emissions. Additionally, Figure 14a illustrates the average objective values obtained with FCFS schedules. Detailed per-instance results are available in Appendix A.

Dataset	% GHG reduction		
	min	mean	max
CAS-MA-PFSP-M1T1	0.83	24.27	70.29
CAS-MA-PFSP-M1T3	5.77	33.04	69.78
CAS-MA-PFSP-M3T1	2.69	19.94	67.60
CAS-MA-PFSP-M3T3	2.35	29.54	64.01

Table 7: Overview of GHG emissions reduction with CAS-MA against FCFS

The results indicate that carbon-aware scheduling consistently reduces GHG emissions across all datasets, with substantial average reductions up to more than 30% when compared to FCFS, one of the most commonly adopted scheduling strategies. This demonstrates the effectiveness of the proposed approach in achieving the primary objective of this study: reducing GHG emissions in manufacturing by leveraging time-dependent grid carbon intensity and on-site renewable generation.

5 Conclusion

In this study, we have developed an efficient tool for aligning power consumption in manufacturing with the time-dependent carbon intensity of the grid and the availability of on-site renewable electricity, thereby reducing scope 2 GHG emissions.

The carbon-aware scheduling model was introduced in Section 2, where we first outlined how grid carbon intensity can be derived from the generation mix and then formulated the scheduling problem as an MILP. Given the NP-hardness of the problem, we proposed a novel memetic algorithm in Section 3 capable of efficiently finding high-quality solutions on real-world-sized instances by combining evolutionary computing with local search. Finally, in Section 4, we conducted computational experiments to evaluate the proposed approach by first discussing instance generation, then the performance evaluation metrics, and finally the experimental results.

Experiments were conducted by running the novel MA-CAS-PFSP algorithm and the CPLEX implementation of the MILP model on four instance datasets of increasing complexity. The results demonstrate consistent GHG emissions reductions across all datasets, averaging up to more than 30% less scope 2 emissions than FCFS schedules. Moreover, the proposed MA algorithm outperforms CPLEX both in terms

of solution quality and computation times on real-world sized instances.

These findings highlight three key contributions of this study. First, they demonstrate how carbon-aware scheduling effectively reduces GHG emissions in manufacturing by leveraging the time-dependent grid carbon intensity and on-site renewable generation. Additionally, the model considers a PFSP manufacturing environment, which resembles how traditional assembly lines are typically built. Finally, the proposed method efficiently solves large-scale instances, making it a well-suited for real-world manufacturing applications.

Despite these contributions, some limitations remain, offering directions for future work. First, while the PFSP environment resembles many traditional assembly lines, it does not fully reflect the flexibility often required in modern manufacturing. With the shift toward high-mix, low-volume production, manufacturers are adopting flexible assembly lines, where job routings can be dynamically adjusted to accommodate product customization. Extending the model to a flexible-job-shop environment (FJSP) would enhance its applicability to contemporary manufacturing systems. Second, the performance of metaheuristics is highly dependent on the values of their parameters, which require careful tuning to achieve good results across instances with similar characteristics. However, energy-related data such as grid carbon intensity and on-site renewable generation can differ significantly from day to day, leading to substantial differences even between similar instances (e.g., same number of jobs, machines, and job power requirements). These day-to-day differences may require frequent re-tuning of parameters, which is impractical for real-world deployment. Moreover, the effectiveness of a parameter setting may change during the search. Future research should explore self-adapting parameter control strategies, enabling the algorithm to dynamically adjust its parameters throughout the search process based on instance characteristics, thereby eliminating the need for manual (re-)tuning. Third, while day-ahead forecasts for energy-related data are widely available, they are inherently uncertain. Moreover, the accuracy of these forecasts diminishes as the time horizon extends. As a result, a schedule that is initially optimal can become suboptimal as new, more accurate data becomes available throughout the planning horizon. To mitigate this issue, future research should integrate real-time information into closed-loop rescheduling algorithms, allowing schedules to adapt dynamically and restore optimality as conditions change.

Acknowledgements

We gratefully acknowledge the financial support provided by the Actemium chair on Sustainable Energy*.

References

- [1] Ahlqvist, V., Holmberg, P., and Tangerås, T. (2022). A survey comparing centralized and decentralized electricity markets. *Energy Strategy Reviews*, 40:100812. DOI: 10.1016/j.esr.2022.100812.

*<https://www.ugent.be/schenken/en/how-to-support/chairs/actemium>

- [2] Ahmadian, M. M., Khatami, M., Salehipour, A., and Cheng, T. (2021). Four decades of research on the open-shop scheduling problem to minimize the makespan. *European Journal of Operational Research*, 295(2):399–426. DOI: 10.1016/j.ejor.2021.03.026.
- [3] Akiba, T., Sano, S., Yanase, T., Ohta, T., and Koyama, M. (2019). Optuna: A next-generation hyperparameter optimization framework. In *Proceedings of the 25th ACM SIGKDD International Conference on Knowledge Discovery & Data Mining*, KDD '19, page 2623–2631, New York, NY, USA. Association for Computing Machinery. DOI: 10.1145/3292500.3330701.
- [4] Baker, K. R. and Trietsch, D. (2018). *Principles of sequencing and scheduling*. John Wiley & Sons. DOI: 10.1002/9780470451793.
- [5] Batalla-Bejerano, J. and Trujillo-Baute, E. (2016). Impacts of intermittent renewable generation on electricity system costs. *Energy Policy*, 94:411–420. DOI: 10.1016/j.enpol.2015.10.024.
- [6] Baumgärtner, N., Delorme, R., Hennen, M., and Bardow, A. (2019). Design of low-carbon utility systems: Exploiting time-dependent grid emissions for climate-friendly demand-side management. *Applied Energy*, 247:755–765. DOI: 10.1016/j.apenergy.2019.04.029.
- [7] Bean, J. C. (1994). Genetic algorithms and random keys for sequencing and optimization. *ORSA journal on computing*, 6(2):154–160. DOI: 10.1287/ijoc.6.2.154.
- [8] Bergstra, J., Bardenet, R., Bengio, Y., and Kégl, B. (2011). Algorithms for hyper-parameter optimization. In *Advances in Neural Information Processing Systems*, volume 24, pages 2546–2554. https://proceedings.neurips.cc/paper_files/paper/2011/file/86e8f7ab32cfd12577bc2619bc635690-Paper.pdf.
- [9] Che, A., Zeng, Y., and Lyu, K. (2016). An efficient greedy insertion heuristic for energy-conscious single machine scheduling problem under time-of-use electricity tariffs. *Journal of Cleaner Production*, 129:565–577. DOI: 10.1016/j.jclepro.2016.03.150.
- [10] Cheng, J., Chu, F., Liu, M., Wu, P., and Xia, W. (2017). Bi-criteria single-machine batch scheduling with machine on/off switching under time-of-use tariffs. *Computers & Industrial Engineering*, 112:721–734. DOI: 10.1016/j.cie.2017.04.026.
- [11] Cheng, R., Gen, M., and Tsujimura, Y. (1999). A tutorial survey of job-shop scheduling problems using genetic algorithms, part ii: hybrid genetic search strategies. *Computers & Industrial Engineering*, 36(2):343–364. DOI: 10.1016/S0360-8352(99)00136-9.
- [12] Cui, W. and Lu, B. (2021). Energy-aware operations management for flow shops under tou electricity tariff. *Computers & Industrial Engineering*, 151:106942. DOI: 10.1016/j.cie.2020.106942.
- [13] da Jiang, E. and Wang, L. (2020). Multi-objective optimization based on decomposition for flexible job shop scheduling under time-of-use electricity prices. *Knowledge-Based Systems*, 204:106177. DOI: 10.1016/j.knosys.2020.106177.
- [14] Ding, J.-Y., Song, S., and Wu, C. (2016a). Carbon-efficient scheduling of flow shops by multi-objective optimization. *European Journal of Operational Research*, 248(3):758–771. DOI: 10.1016/j.ejor.2015.05.019.
- [15] Ding, J.-Y., Song, S., Zhang, R., Chiong, R., and Wu, C. (2016b). Parallel machine scheduling under time-of-use electricity prices: New models and optimization approaches. *IEEE Transactions on Automation Science and Engineering*, 13(2):1138–1154. DOI: 10.1109/TASE.2015.2495328.
- [16] Dong, J. and Ye, C. (2022). Green scheduling of distributed two-stage reentrant hybrid flow shop considering distributed energy resources and energy storage system. *Computers & Industrial Engineering*, 169:108146. DOI: 10.1016/j.cie.2022.108146.
- [17] Eiben, A. E. and Smith, J. E. (2015). *Introduction to evolutionary computing*. Springer. DOI: 10.1007/978-3-662-44874-8.
- [18] Elia (2025a). *Day-ahead schedule of power generation - aggregated by fuel type - data up to 22/05/2024*. Open Data Platform. <https://opendata.elia.be/explore/dataset/ods034/information/> Accessed: 2025-01-08.
- [19] Elia (2025b). *Photovoltaic power production estimation and forecast on Belgian grid (Historical)*. Open Data Platform. <https://opendata.elia.be/explore/dataset/ods032/information/> Accessed: 2025-01-08.
- [20] European Commission and Directorate-General for Climate Action (2019). *Going climate-neutral by 2050 – A strate-*

gic long-term vision for a prosperous, modern, competitive and climate-neutral EU economy. Publications Office of the European Union. DOI: 10.2834/02074.

- [21] European Commission: Eurostat (2023 interactive publication). *Shredding light on energy in the EU.* Publications Office of the European Union. DOI: 10.2785/405482.
- [22] European Environment Agency (2023). *Trends and projections in Europe 2023.* Publications Office of the European Union. DOI: 10.2800/595102.
- [23] European Union: European Commission (1 February 2023, COM(2023) 62 final). *Communication from the Commission to the European Parliament, the European Council, the Council, the European Economic and Social Committee and the Committee of the Regions: A Green Deal Industrial Plan for the Net-Zero Age.* The European Commission. <https://eur-lex.europa.eu/legal-content/EN/TXT/?uri=CELEX%3A52023DC0062&qid=1678874483913>.
- [24] Fallahi, A., Shahidi-Zadeh, B., and Niaki, S. T. A. (2023). Unrelated parallel batch processing machine scheduling for production systems under carbon reduction policies: Nsga-ii and mogwo metaheuristics. *Soft Computing*, 27(22):17063–17091. DOI: 10.1007/s00500-023-08754-0.
- [25] Fazli Khalaf, A. and Wang, Y. (2018). Energy-cost-aware flow shop scheduling considering intermittent renewables, energy storage, and real-time electricity pricing. *International Journal of Energy Research*, 42(12):3928–3942. DOI: 10.1002/er.4130.
- [26] Fernandez-Viagas, V., Ruiz, R., and Framinan, J. M. (2017). A new vision of approximate methods for the permutation flowshop to minimise makespan: State-of-the-art and computational evaluation. *European Journal of Operational Research*, 257(3):707–721. DOI: 10.1016/j.ejor.2016.09.055.
- [27] Garey, M. R., Johnson, D. S., and Sethi, R. (1976). The complexity of flowshop and jobshop scheduling. *Mathematics of Operations Research*, 1(2):117–129. DOI: 10.1287/moor.1.2.117.
- [28] Ghorbani Saber, R. and Ranjbar, M. (2022). Minimizing the total tardiness and the total carbon emissions in the permutation flow shop scheduling problem. *Computers & Operations Research*, 138:105604. DOI: 10.1016/j.cor.2021.105604.
- [29] Ghorbanzadeh, M. and Ranjbar, M. (2023). Energy-aware production scheduling in the flow shop environment under sequence-dependent setup times, group scheduling and renewable energy constraints. *European Journal of Operational Research*, 307(2):519–537. DOI: 10.1016/j.ejor.2022.09.034.
- [30] Greenhouse Gas Protocol (2004). *A Corporate Accounting and Reporting Standard.* World Resources Institute and World Business Council for Sustainable Development. <https://ghgprotocol.org/sites/default/files/standards/ghg-protocol-revised.pdf>.
- [31] Greenhouse Gas Protocol (2015). *GHG Protocol Scope 2 Guidance.* WRI: World Resources Institute. <https://ghgprotocol.org/sites/default/files/2023-03/Scope%20%20Guidance.pdf>.
- [32] Ho, M. H., Hnaien, F., and Dugardin, F. (2022). Exact method to optimize the total electricity cost in two-machine permutation flow shop scheduling problem under time-of-use tariff. *Computers & Operations Research*, 144:105788. DOI: 10.1016/j.cor.2022.105788.
- [33] Holland, S. P. and Mansur, E. T. (2008). Is Real-Time Pricing Green? The Environmental Impacts of Electricity Demand Variance. *The Review of Economics and Statistics*, 90(3):550–561. DOI: 10.1162/rest.90.3.550.
- [34] IEA (2022). *Electricity Market Report - January 2022.* International Energy Agency, Paris. <https://www.iea.org/reports/electricity-market-report-january-2022>.
- [35] Intergovernmental Panel on Climate Change (2015). Technology-specific cost and performance parameters. In *Climate Change 2014: Mitigation of Climate Change: Working Group III Contribution to the IPCC Fifth Assessment Report*, page 1329–1356. Cambridge University Press. DOI: 10.1017/CBO9781107415416.
- [36] Intergovernmental Panel on Climate Change (2023). *Climate Change 2023: Synthesis Report. Contribution of Working Groups I, II and III to the Sixth Assessment Report of the Intergovernmental Panel on Climate Change.* IPCC, Geneva, Switzerland, pp. 35-115. DOI: 10.59327/IPCC/AR6-9789291691647.
- [37] Karimi, S. and Kwon, S. (2021). Comparative analysis of the impact of energy-aware scheduling, renewable energy generation, and battery energy storage on production scheduling. *International Journal of Energy Research*, 45(13):18981–

18998. DOI: 10.1002/er.6999.

- [38] Kelley, M. T., Baldick, R., and Baldea, M. (2018). Demand response operation of electricity-intensive chemical processes for reduced greenhouse gas emissions: application to an air separation unit. *ACS Sustainable Chemistry & Engineering*, 7(2):1909–1922. DOI: 10.1021/acssuschemeng.8b03927.
- [39] Kopsakangas-Savolainen, M., Mattinen, M. K., Manninen, K., and Nissinen, A. (2017). Hourly-based greenhouse gas emissions of electricity – cases demonstrating possibilities for households and companies to decrease their emissions. *Journal of Cleaner Production*, 153:384–396. DOI: j.jclepro.2015.11.027.
- [40] Liu, C.-H. (2016). Mathematical programming formulations for single-machine scheduling problems while considering renewable energy uncertainty. *International Journal of Production Research*, 54(4):1122–1133. DOI: 10.1080/00207543.2015.1048380.
- [41] Liu, Q., Zhan, M., Chekem, F. O., Shao, X., Ying, B., and Sutherland, J. W. (2017). A hybrid fruit fly algorithm for solving flexible job-shop scheduling to reduce manufacturing carbon footprint. *Journal of Cleaner Production*, 168:668–678. DOI: 10.1016/j.jclepro.2017.09.037.
- [42] Londe, M. A., Pessoa, L. S., Andrade, C. E., and Resende, M. G. (2025). Biased random-key genetic algorithms: A review. *European Journal of Operational Research*, 321(1):1–22. DOI: 10.1016/j.ejor.2024.03.030.
- [43] Luo, H., Du, B., Huang, G. Q., Chen, H., and Li, X. (2013). Hybrid flow shop scheduling considering machine electricity consumption cost. *International Journal of Production Economics*, 146(2):423–439. DOI: 10.1016/j.ijpe.2013.01.028.
- [44] Miller, G. J., Novan, K., and Jenn, A. (2022). Hourly accounting of carbon emissions from electricity consumption. *Environmental Research Letters*, 17(4). DOI: 10.1088/1748-9326/ac6147.
- [45] Minh Hung Ho, F. H. and Dugardin, F. (2021). Electricity cost minimisation for optimal makespan solution in flow shop scheduling under time-of-use tariffs. *International Journal of Production Research*, 59(4):1041–1067. DOI: 10.1080/00207543.2020.1715504.
- [46] Moon, J.-Y. and Park, J. (2014). Smart production scheduling with time-dependent and machine-dependent electricity cost by considering distributed energy resources and energy storage. *International Journal of Production Research*, 52(13):3922–3939. DOI: 10.1080/00207543.2013.860251.
- [47] Moon, J.-Y., Shin, K., and Park, J. (2013). Optimization of production scheduling with time-dependent and machine-dependent electricity cost for industrial energy efficiency. *The International Journal of Advanced Manufacturing Technology*, 68:523–535. DOI: 10.1007/s00170-013-4749-8.
- [48] Ostermeier, F. F. and Deuse, J. (2024). A review and classification of scheduling objectives in unpaced flow shops for discrete manufacturing. *Journal of Scheduling*, 27(1):29–49. DOI: 10.1007/s10951-023-00795-5.
- [49] Oukil, A., El-Bouri, A., and Emrouznejad, A. (2022). Energy-aware job scheduling in a multi-objective production environment – an integrated dea-owa model. *Computers & Industrial Engineering*, 168:108065. DOI: 10.1016/j.cie.2022.108065.
- [50] Pinedo, M. L. (2022). *Scheduling: Theory, Algorithms, and Systems*. Springer Cham. DOI: 10.1007/978-3-031-05921-6.
- [51] Rubaiee, S. and Yildirim, M. B. (2019). An energy-aware multiobjective ant colony algorithm to minimize total completion time and energy cost on a single-machine preemptive scheduling. *Computers & Industrial Engineering*, 127:240–252. DOI: 10.1016/j.cie.2018.12.020.
- [52] Shen, K., De Pessemier, T., Martens, L., and Joseph, W. (2021). A parallel genetic algorithm for multi-objective flexible flowshop scheduling in pasta manufacturing. *Computers & Industrial Engineering*, 161:107659. DOI: 10.1016/j.cie.2021.107659.
- [53] Shen, L., Dauzère-Pérès, S., and Maecker, S. (2023). Energy cost efficient scheduling in flexible job-shop manufacturing systems. *European Journal of Operational Research*, 310(3):992–1016. DOI: 10.1016/j.ejor.2023.03.041.
- [54] Soares, L. C. R. and Carvalho, M. A. M. (2020). Biased random-key genetic algorithm for scheduling identical parallel machines with tooling constraints. *European Journal of Operational Research*, 285(3):955–964. DOI: 10.1016/j.ejor.2020.02.047.
- [55] Tian, Z. and Zheng, L. (2024). Single machine parallel-batch scheduling under time-of-use electricity prices:

New formulations and optimisation approaches. *European Journal of Operational Research*, 312(2):512–524. DOI: 10.1016/j.ejor.2023.07.012.

- [56] Trevino-Martinez, S., Sawhney, R., and Shylo, O. (2022a). Energy-carbon footprint optimization in sequence-dependent production scheduling. *Applied Energy*, 315:118949. DOI: 10.1016/j.apenergy.2022.118949.
- [57] Trevino-Martinez, S., Sawhney, R., and Sims, C. (2022b). Energy-carbon neutrality optimization in production scheduling via solar net metering. *Journal of Cleaner Production*, 380:134627. DOI: 10.1016/j.jclepro.2022.134627.
- [58] Wang, S., Zhu, Z., Fang, K., Chu, F., and Chu, C. (2018). Scheduling on a two-machine permutation flow shop under time-of-use electricity tariffs. *International Journal of Production Research*, 56(9):3173–3187. DOI: 10.1080/00207543.2017.1401236.
- [59] Wolpert, D. and Macready, W. (1997). No free lunch theorems for optimization. *IEEE Transactions on Evolutionary Computation*, 1(1):67–82. DOI: 10.1109/4235.585893.
- [60] Zhang, H., Zhao, F., Fang, K., and Sutherland, J. W. (2014). Energy-conscious flow shop scheduling under time-of-use electricity tariffs. *CIRP Annals*, 63(1):37–40. DOI: 10.1016/j.cirp.2014.03.011.

Appendix A Detailed results per instance

n	MA				CPLEX		MA vs CPLEX	MA vs FCFS	
	best	mean	cv	mean time (s)	obj.	time (s)	% Δ	obj.	% Δ
1	6308572	6310871	5.88×10^{-4}	0.87	6307956	2.92	-9.77×10^{-3}	7496109	15.84
2	6023265	6023265	0.00	0.82	6023265	2.22	0.00	6168539	2.36
3	31385145	31393590	4.00×10^{-4}	1.11	31385145	5.78	0.00	33316107	5.8
4	12671207	12671207	0.00	0.90	12671207	2.59	0.00	14302310	11.4
5	4926132	4926132	0.00	0.90	4926132	0.92	0.00	13287933	62.93
6	9775079	9776279	3.68×10^{-4}	0.82	9775079	3.58	0.00	10244460	4.58
7	12685460	12686132	1.59×10^{-4}	0.82	12685460	6.82	0.00	13136016	3.43
8	4025550	4029583	1.46×10^{-3}	0.88	4025550	4.67	0.00	6316635	36.27
9	7816029	7818598	3.29×10^{-4}	0.92	7816029	3.81	0.00	8959726	12.76
10	13986714	13986714	0.00	0.90	13986714	2.72	0.00	15871294	11.87
11	11083051	11084495	8.53×10^{-5}	0.89	11083051	2.40	0.00	17568920	36.92
12	3544280	3546722	3.46×10^{-4}	0.83	3544280	0.74	0.00	7907626	55.18
13	4123336	4123336	0.00	0.96	4123336	7.33	0.00	7996723	48.44
14	7806568	7822820	1.94×10^{-3}	0.74	7806568	0.66	0.00	9129390	14.49
15	4364419	4364520	2.32×10^{-5}	0.82	4363582	4.95	-1.92×10^{-2}	5713884	23.62
16	9842727	9843291	1.15×10^{-4}	0.83	9842727	1.16	0.00	9972696	1.30
17	10358284	10358284	0.00	0.82	10358284	12.12	0.00	10473047	1.10
18	6332015	6332187	2.62×10^{-5}	0.89	6332015	2.27	0.00	6545293	3.26
19	4300170	4301172	6.99×10^{-4}	1.04	4300170	6.23	0.00	7850134	45.22
20	5940690	5975584	8.46×10^{-3}	1.12	5940690	14.90	0.00	14963388	60.30
21	7786894	7787077	4.70×10^{-5}	0.82	7786894	1.67	0.00	9086649	14.30
22	4775334	4792098	3.52×10^{-3}	1.03	4775334	5.26	0.00	6913598	30.93
23	10401049	10401049	0.00	1.01	10401049	2.54	0.00	11999826	13.32
24	6495650	6532657	2.51×10^{-3}	0.85	6495650	1.16	0.00	7805278	16.78
25	1577204	1600001	9.33×10^{-3}	0.85	1577204	2.77	0.00	5021615	68.59
26	9266737	9293534	4.51×10^{-3}	0.91	9266737	0.88	0.00	14162970	34.57
27	3134368	3143093	2.27×10^{-3}	0.95	3134368	2.29	0.00	5261344	40.43
28	1827219	1843400	1.83×10^2	0.80	1827219	0.81	0.00	6150914	70.29
29	2421790	2426410	2.10×10^{-3}	0.84	2421790	0.53	0.00	4229224	42.74
30	13179003	13179003	0.00	0.97	13179003	3.54	0.00	21746561	39.40
31	3912915	3936309	7.41×10^{-3}	0.92	3912915	0.72	0.00	6806802	42.51
32	11728357	11730500	3.04×10^{-4}	1.09	11728357	4.97	0.00	12557585	6.60
33	6442129	6442217	1.11×10^{-5}	1.19	6442129	4.86	0.00	6559518	1.79
34	14244214	14245272	1.13×10^{-4}	1.10	14244214	3.06	0.00	15322370	7.04
35	4887613	4916667	1.10×10^2	0.99	4887613	5.43	0.00	15694827	68.86
36	9881006	9885155	2.82×10^{-4}	1.16	9877924	9.81	-3.12×10^{-2}	10272078	3.81
37	5886606	5930329	9.29×10^{-3}	1.32	5886606	7.97	0.00	11453759	48.61
38	8349826	8349834	3.05×10^{-6}	0.91	8349826	3.85	0.00	10797146	22.67
39	18313071	18317344	5.30×10^{-4}	1.00	18313071	3.03	0.00	20246059	9.55
40	10748301	10773716	3.25×10^{-3}	1.00	10748301	5.90	0.00	11956411	10.10
41	18946131	18967056	8.32×10^{-4}	1.43	18946131	7.37	0.00	21155899	10.45
42	6515369	6531141	1.39×10^{-3}	1.26	6515369	13.98	0.00	10630141	38.71
43	9817039	9825997	4.28×10^{-4}	0.98	9817039	3.65	0.00	10217483	3.92
44	5338081	5346834	2.57×10^{-3}	0.91	5338081	1.14	0.00	6894334	22.57
45	7346877	7346877	0.00	1.06	7346877	32.85	0.00	8152295	9.88
46	7307368	7308487	1.87×10^{-4}	0.95	7307368	4.11	0.00	7368464	0.83
47	4643796	4643796	0.00	0.61	4643796	0.20	0.00	5399076	13.99
48	7108511	7108511	0.00	0.92	7108511	5.19	0.00	9022732	21.22
49	5299673	5301078	4.11×10^{-4}	0.86	5299673	6.92	0.00	8454863	37.32
50	6056698	6066832	2.87×10^{-3}	0.92	6056698	4.13	0.00	6337218	4.43
\bar{n}	8219337	8227276	1.91×10^{-3}	0.95	8218660	4.79	-1.20×10^{-3}	10697945	24.27

Table 8: Detailed results for the CAS-PFSP-M1T1 dataset

n	MA				CPLEX		MA vs CPLEX	MA vs FCFS	
	best	mean	cv	mean time (s)	obj.	time (s)	% Δ	obj.	% Δ
1	16821461	16929195	6.02×10^{-3}	2.34	22702306	60	25.90	25562356	34.19
2	22878800	23006105	3.69×10^{-3}	2.42	24934642	60	8.24	28985090	21.07
3	17166947	17499914	1.19×10^{-2}	2.14	30613796	60	43.92	30613796	43.92
4	59409585	59845550	4.24×10^{-3}	2.4	60202390	60	1.32	71788748	17.24
5	22838354	23395977	1.41×10^{-2}	2.42	34142943	60	33.11	36687017	37.75
6	48307535	48602496	4.04×10^{-3}	2.07	57776078	60	16.39	58046716	16.78
7	37742526	37939529	3.48×10^{-3}	2.42	42772764	60	11.76	42772764	11.76
8	11396303	11699656	1.52×10^{-2}	2.39	13781562	60	17.31	25631271	55.54
9	15293363	15563490	9.01×10^{-3}	2.34	17786101	60	14.02	24144030	36.66
10	47325893	47696278	7.19×10^{-3}	2.34	49869433	60	5.10	70863895	33.22
11	14574193	14662711	3.43×10^{-3}	2.16	14796995	60	1.51	18752164	22.28
12	11631372	11952703	2.30×10^{-2}	2.28	18165231	60	35.97	21054319	44.76
13	25144894	25435945	7.39×10^{-3}	2.53	28664870	60	12.28	39256506	35.95
14	14861636	15102037	1.09×10^{-2}	2.72	27751662	60	46.45	27755705	46.46
15	79077915	79380660	2.07×10^{-3}	2.37	80975698	60	2.34	89398936	11.54
16	20121229	21125460	2.55×10^{-2}	2.97	39296479	60	48.80	39296479	48.80
17	10168679	10437837	1.88×10^{-2}	2.19	18149158	60	43.97	22528710	54.86
18	15354274	15633261	1.00×10^{-2}	2.4	24085948	60	36.25	33478873	54.14
19	17156408	17428688	1.11×10^{-2}	2.86	25651923	60	33.12	29086099	41.02
20	22117354	22417905	8.13×10^{-3}	2.88	33888193	60	34.73	33888193	34.73
21	21771038	22282636	1.73×10^{-2}	2.98	27012304	60	19.40	41419873	47.44
22	14747399	14988233	1.14×10^{-2}	3.03	17396195	60	15.23	33748491	56.30
23	16721243	16945709	8.19×10^{-3}	3.15	25153585	60	33.52	25153585	33.52
24	15822410	15880617	2.07×10^{-3}	2.41	16280388	60	2.81	17466683	9.41
25	12351610	12487238	8.60×10^{-3}	2.62	13099170	60	5.71	23640187	47.75
26	16872978	17413205	2.70×10^{-2}	2.55	35184700	60	52.04	35184700	52.04
27	11848197	12277525	1.79×10^{-2}	2.94	29860146	60	60.32	32715617	63.78
28	6189632	6491788	3.23×10^{-2}	2.52	8372272	60	26.07	20481785	69.78
29	20240421	20391040	4.99×10^{-3}	2.61	20914152	60	3.22	25039066	19.16
30	15860100	16430952	2.15×10^{-2}	2.33	31996300	60	50.43	31996300	50.43
31	23311288	23730203	9.65×10^{-3}	2.46	32762652	60	28.85	37039733	37.06
32	26713621	27164166	1.45×10^{-2}	2.43	32054580	60	16.66	37710540	29.16
33	16976117	17120560	5.85×10^{-3}	3.2	17311270	60	1.94	19748840	14.04
34	22110616	22283264	5.64×10^{-3}	3	28752129	60	23.10	28759593	23.12
35	17641565	18146257	1.59×10^{-2}	4.84	26784312	60	34.13	27549279	35.96
36	19915092	20450260	1.59×10^{-2}	2.86	26709199	60	25.44	44564534	55.31
37	19851873	20356986	1.45×10^{-2}	2.87	26857845	60	26.09	26857845	26.09
38	22667578	22896470	5.92×10^{-3}	2.76	23500668	60	3.54	33164212	31.65
39	15125275	15247881	6.76×10^{-3}	2.73	16617329	60	8.98	20200140	25.12
40	20302253	20411332	2.28×10^{-3}	2.26	21739739	60	6.61	24642430	17.61
41	13257406	13317086	3.05×10^{-3}	2.53	14660229	60	9.57	15776795	15.97
42	26686990	26715347	8.75×10^{-4}	2.43	28992793	60	7.95	37289967	28.43
43	27161932	27575990	8.42×10^{-3}	3.13	36749365	60	26.09	36749365	26.09
44	32061593	32130066	1.43×10^{-3}	2.56	33810231	60	5.17	36333565	11.76
45	30787021	30973681	3.94×10^{-3}	2.78	37474522	60	17.85	37474522	17.85
46	28474944	28553967	2.21×10^{-3}	2.78	31855648	60	10.61	36203951	21.35
47	20789953	20829157	1.25×10^{-3}	2.63	21386634	60	2.79	22064130	5.77
48	16834188	17065499	8.21×10^{-3}	2.04	19708832	60	14.59	26092462	35.48
49	41177069	41309892	2.80×10^{-3}	2.53	41727298	60	1.32	49492588	16.80
50	17830456	18041256	8.19×10^{-3}	2.95	19160643	60	6.94	23801838	25.09
\bar{n}	22829812	23113273	9.76×10^{-3}	2.63	28597866	60	20.39	33559086	33.04

Table 9: Detailed results for the CAS-PFSP-M1T3 dataset

n	MA				CPLEX		MA vs CPLEX	MA vs FCFS	
	best	mean	cv	mean time (s)	obj.	time (s)	% Δ	obj.	% Δ
1	19411107	19710360	1.47×10^{-2}	6.59	20494190	60	5.28	23561761	17.62
2	6824449	6843679	1.92×10^{-3}	5.75	6815486	60	-0.13	7260127	6.00
3	10854363	10952014	5.96×10^{-3}	7.61	11753527	60	7.65	13209616	17.83
4	30266452	30447558	6.77×10^{-3}	8.64	37994870	60	20.34	37878976	20.10
5	7320599	7444914	1.37×10^{-2}	5.77	8137794	60	10.04	13507427	45.80
6	19151404	19390912	7.16×10^{-3}	6.62	19702255	60	2.80	25764606	25.67
7	13873227	13916474	2.41×10^{-3}	6.74	14394557	60	3.62	14606611	5.02
8	7685950	7744345	4.67×10^{-3}	8.17	8528573	60	9.88	9098369	15.52
9	17405672	17477728	2.97×10^{-3}	8.68	19022523	60	8.50	19327936	9.95
10	6696758	6708221	1.23×10^{-3}	6.16	6920900	60	3.24	7491587	10.61
11	9073324	9245238	1.33×10^{-2}	6.76	9528843	60	4.78	11603613	21.81
12	34798297	35157267	1.09×10^{-2}	7.07	35518431	60	2.03	39168864	11.16
13	23289338	23562654	7.35×10^{-3}	4.97	22816375	60	-2.07	29945761	22.23
14	31529076	31659889	4.68×10^{-3}	6.11	31820590	60	0.92	33719562	6.50
15	9453699	9548974	6.61×10^{-3}	7.7	9539872	60	0.90	12007971	21.27
16	21017028	21341069	1.22×10^{-2}	6.13	22032950	60	4.61	24413362	13.91
17	13942310	14125539	6.94×10^{-3}	7.22	15402540	60	9.48	15686054	11.12
18	9804851	9852377	4.00×10^{-3}	7.19	10909275	60	10.12	10872948	9.82
19	8155899	8166078	9.26×10^{-4}	6.73	8219804	60	0.78	8381536	2.69
20	9105858	9116584	1.51×10^{-3}	7.18	10575124	60	13.89	10619377	14.25
21	10493966	10520989	1.66×10^{-3}	6.45	11001841	60	4.62	11389435	7.86
22	19376072	19564093	6.27×10^{-3}	6.64	20679402	60	6.30	28224950	31.35
23	7098481	7161596	5.29×10^{-3}	6.7	8354496	60	15.03	9482649	25.14
24	35892401	36206052	4.30×10^{-3}	9.59	40824703	60	12.08	40668769	11.74
25	13232793	13300529	3.48×10^{-3}	5.74	13214197	60	-0.14	14324173	7.62
26	10107294	10136972	1.65×10^{-3}	7.81	11023475	60	8.31	11119811	9.11
27	41658645	41855183	2.82×10^{-3}	6.85	42529624	60	2.05	46752546	10.90
28	27926607	28045671	3.49×10^{-3}	8.36	29882686	60	6.55	29713037	6.01
29	8016708	8142503	1.11×10^{-2}	5.13	8186679	60	2.08	16712006	52.03
30	12319959	12651949	2.02×10^{-2}	6.64	18626562	60	33.86	26796753	54.02
31	21002543	21096017	3.70×10^{-3}	7.98	22890195	60	8.25	26192881	19.82
32	37294205	37461059	3.57×10^{-3}	6.4	37992649	60	1.84	43112751	13.50
33	24574292	24641180	1.94×10^{-3}	6.49	25021164	60	1.79	27263728	9.86
34	8723462	8742500	1.70×10^{-3}	7.95	10381645	60	15.97	10674061	18.27
35	15028940	15149878	6.39×10^{-3}	7.87	18857519	60	20.30	21305695	29.46
36	10723509	10767171	2.63×10^{-3}	9.45	12111752	60	11.46	11967630	10.40
37	23605525	23839759	6.36×10^{-3}	8.32	24655408	60	4.26	25732236	8.26
38	4212519	4273191	1.26×10^{-2}	7.48	6843342	60	38.44	7060375	40.34
39	12350759	12375550	1.25×10^{-3}	6.47	12392681	60	0.34	13518670	8.64
40	7239889	7628380	4.60×10^{-2}	6.65	14539319	60	50.20	22344612	67.60
41	12587406	12613361	1.00×10^{-3}	6.77	12618938	60	0.25	13683494	8.01
42	9486340	9518515	4.87×10^{-3}	6.48	9524031	60	0.40	12699812	25.30
43	3644229	3864575	3.18×10^{-2}	6.48	4217468	60	13.59	10358982	64.82
44	29710506	30342083	1.22×10^{-2}	6.26	30654143	60	3.08	35348636	15.95
45	9294455	9302656	8.61×10^{-4}	8.04	10644627	60	12.68	12237271	24.05
46	6889245	7042110	1.79×10^{-2}	5.25	8651045	60	20.37	17234890	60.03
47	9055629	9080488	1.22×10^{-3}	7.56	9852672	60	8.09	9801985	7.61
48	21308205	21536370	5.25×10^{-3}	7.6	22699255	60	6.13	23220215	8.23
49	9535492	9553728	1.24×10^{-3}	4.96	9529816	60	-0.06	10203447	6.55
50	6529055	6591481	6.75×10^{-3}	8.19	8461479	60	22.84	8798142	25.79
\bar{n}	15571576	15708349	7.19×10^{-3}	7.01	16939826	60	8.95	19321394	19.94

Table 10: Detailed results for the CAS-PFSP-M3T1 dataset

n	MA				CPLEX		MA vs CPLEX	MA vs FCFS	
	best	mean	cv	mean time (s)	obj.	time (s)	% Δ	obj.	% Δ
1	26197048	27047173	2.65×10^{-2}	17.92	31588004	60	17.07	31588004	17.07
2	30017723	30610970	1.36×10^{-2}	18.49	77794570	60	61.41	77794570	61.41
3	88010952	89699983	1.44×10^{-2}	25.6	138422552	60	36.42	138422552	36.42
4	62164808	63712935	1.35×10^{-2}	21.91	100350390	60	38.05	100350390	38.05
5	34451497	35351110	1.79×10^{-2}	22.35	60213959	60	42.78	60213959	42.78
6	74716810	76183056	1.26×10^{-2}	27.57	109243882	60	31.61	109243882	31.61
7	46746880	47964291	2.25×10^{-2}	19.98	70125167	60	33.34	70125167	33.34
8	15032309	16561977	5.38×10^{-2}	19.68	41767533	60	64.01	41767533	64.01
9	115635395	116899594	8.74×10^{-3}	27.24	141153050	60	18.08	141153050	18.08
10	53564544	53711220	2.54×10^{-3}	26.34	60764811	60	11.85	60764811	11.85
11	43002369	43091686	1.89×10^{-3}	29.01	49238557	60	12.67	49238557	12.67
12	24800939	25959121	2.86×10^{-2}	20.7	51171649	60	51.53	51171649	51.53
13	29183840	29650086	1.15×10^{-2}	20.22	35525105	60	17.85	35525105	17.85
14	86351782	87168019	5.21×10^{-3}	23.51	101642666	60	15.04	101642666	15.04
15	71921556	73012231	7.24×10^{-3}	24.9	109555882	60	34.35	109555882	34.35
16	42691782	43541999	1.62×10^{-2}	21.79	54368510	60	21.48	54368510	21.48
17	43467534	47126996	3.61×10^{-2}	18.21	98292848	60	55.78	98292848	55.78
18	40630724	41753210	1.36×10^{-2}	24.67	61485903	60	33.92	61485903	33.92
19	33117841	33750223	1.37×10^{-2}	19.49	51613353	60	35.83	51613353	35.83
20	66785458	67539456	9.00×10^{-3}	28.02	81795726	60	18.35	81795726	18.35
21	39987448	40146832	1.95×10^{-3}	23.98	41976357	60	4.74	41976357	4.74
22	47127909	48399883	1.95×10^{-2}	26.92	78055888	60	39.62	78055888	39.62
23	32058547	32906555	1.37×10^{-2}	23.68	62854938	60	49.00	62854938	49.00
24	39293038	39933642	8.36×10^{-3}	25.62	51873180	60	24.25	51873180	24.25
25	70498459	70880027	3.01×10^{-3}	25.03	76235061	60	7.52	76235061	7.52
26	53793951	54208023	7.61×10^{-3}	26.56	72650068	60	25.95	72650068	25.95
27	36847699	37158213	4.93×10^{-3}	22.87	43338685	60	14.98	43338685	14.98
28	38027768	38768700	1.29×10^{-2}	25.93	55268688	60	31.19	55268688	31.19
29	74760673	76121591	1.14×10^{-2}	18.74	92352667	60	19.05	92352667	19.05
30	27661121	28515815	2.22×10^{-2}	20.31	55070803	60	49.77	55070803	49.77
31	21442029	23213866	5.23×10^{-2}	19.1	52181829	60	58.91	52181829	58.91
32	30299871	30716442	8.52×10^{-3}	20.57	38898530	60	22.11	38898530	22.11
33	32560392	33811493	1.92×10^{-2}	20.79	52731799	60	38.25	52731799	38.25
34	30371437	30648687	5.79×10^{-3}	23.18	36780351	60	17.42	36780351	17.42
35	43917542	44285381	5.18×10^{-3}	18.22	49557636	60	11.38	49557636	11.38
36	54993990	56032145	7.76×10^{-3}	19.3	63004293	60	12.71	63004293	12.71
37	39647946	40374724	1.10×10^{-2}	25.81	56768542	60	30.16	56768542	30.16
38	40783100	41750483	1.70×10^{-2}	19.88	60475353	60	32.56	60475353	32.56
39	51692359	52860991	1.03×10^{-2}	26.45	85361666	60	39.44	85361666	39.44
40	122952034	123722402	4.15×10^{-3}	19.14	146484810	60	16.06	146484810	16.06
41	52532207	54096091	2.07×10^{-2}	21.35	105430918	60	50.17	105430918	50.17
42	33466126	33894222	8.17×10^{-3}	21.19	44226096	60	24.33	44226096	24.33
43	64512575	65856313	8.09×10^{-3}	24.23	95096102	60	32.16	95096102	32.16
44	39396047	42041714	4.05×10^{-2}	18.69	77018838	60	48.85	77018838	48.85
45	43569212	43744740	2.77×10^{-3}	25.63	52077658	60	16.34	52077658	16.34
46	47200018	48152987	9.49×10^{-3}	24.94	81067448	60	41.78	81067448	41.78
47	43930762	44014214	1.07×10^{-3}	20.15	46125591	60	4.76	46125591	4.76
48	30997193	31029640	7.29×10^{-4}	21.4	31743972	60	2.35	31743972	2.35
49	53030101	53820501	9.24×10^{-3}	21	69079802	60	23.23	69079802	23.23
50	63561256	65945258	1.47×10^{-2}	23.4	100466587	60	36.73	100466587	36.73
\bar{n}	48588092	49547738	1.38×10^{-2}	22.63	70007365	60	29.54	70007365	29.54

Table 11: Detailed results for the CAS-PFSP-M3T3 dataset